Construction and Building Materials 490 (2025) 142627

Contents lists available at ScienceDirect

Construction and Building Materials

journal homepage: www.elsevier.com/locate/conbuildmat

A generalised analytical solution for the debonding prediction of FRP-to-substrate joints with different anchorage systems

Hugo C. Biscaia [a,b]

[a] UNIDEMI, Department of Mechanical and Industrial Engineering, NOVA School of Science and Technology, Caparica 2829-516, Portugal
[b] Laboratório Associado de Sistemas Inteligentes, LASI, Guimarães 4800-058, Portugal

ARTICLE INFO

Keywords:
FRP composites
Numerical modelling
Debonding process
Anchorages
Single-lap shear test

ABSTRACT

A generalised analytical model (GAM) is proposed for the debonding simulation of several bonded joints with dissimilar materials, particularly between fibre-reinforced polymer (FRP) and a structural material (e.g., concrete, steel, timber, or clay brick) with or without additional anchorages such as transversely compressed mechanical anchorage, FRP U-jackets, and FRP spike anchors, among others. These anchorages are simulated using axial springs that can exhibit linear or nonlinear behaviour and can be placed anywhere on the bonded joint, i.e., they can be used as an end or loaded anchorage, or placed somewhere between the FRP-loaded and unloaded ends. However, to define the springs, the corresponding load-displacement curves for each anchorage must be known beforehand. Nevertheless, if the local bond behaviour of the anchorage is known, a simple numerical strategy is proposed to estimate the load-displacement of the anchorage. This work considers a series of generated cases covering a wide range of situations. The results obtained from the GAM are compared with those obtained from a commercial finite element package, allowing validation. Several studies found in the literature were also analytically reproduced using the GAM. The analytical results were sufficiently close to the numerical and experimental data, regardless of the anchorage type (with linear or nonlinear load-displacement behaviour), or the location of installation along the bonded length. The mainstream results obtained from the Integral Absolute Error (IAE) were lower than 5 %. All results attested to the good accuracy, potential and versatility of the GAM to be considered and used in the future design of adhesively bonded structures.

1. Introduction

Despite being a long-established technique, bonding two distinct materials with an adhesive has grown immensely in recent decades due to the increase in knowledge of the bond performance of such structures. When bonding a carbon fibre reinforced polymer (CFRP) onto a structural material, adding a primordial material such as the CFRP composite to a damaged structure has important economic, environmental and societal impacts [1]. For instance, instead of demolishing existing structures that have become damaged, the use of CFRP composites can restore or even increase the initial strength of the structures with a marginal impact on the original design or architecture of the structure. Therefore, natural resources can be saved, and the workforce is not required to build new structures. Also, CFRP composites have a good strength-to-weight ratio, high corrosion strength, are easy to transport and apply, and are more durable than other conventional materials. However, when externally bonded (EB) onto a structural material, they are prone to prematurely debond from the substrate material, i.e., the CFRP-to-substrate interface debonds when the CFRP strains are lower than the CFRP strain rupture. Also, the maximum CFRP strain reached in each bonded joint varies from joint to joint, which makes quantification difficult.

To bypass the premature debonding associated with CFRP-to-substrate bonded joints, researchers have introduced and tested various anchorages that aim to delay or prevent the premature debonding of the CFRP composite from the substrate. Two anchorage groups can be defined. The first combines the use of additional CFRP sheets with the CFRP-to-substrate joints, while the other uses a metal anchorage (see Fig. 1). The increase of the CFRP width, the CFRP U-jacketing or U-wrapping, CFRP spike anchors, and the continuous reinforcement embedded at ends (CREatE) are four bonding techniques that can be included in the former type of anchorage (see Fig. 1a). The rationale behind the first two examples is to increase the strength of the CFRP-to-substrate joint by increasing the width of the CFRP composite, since it is well-known that the strength of the bonded joints directly increases with the width, e.g. [2–8]. The CFRP U-jacketing or

E-mail address: hb@fct.unl.pt.

https://doi.org/10.1016/j.conbuildmat.2025.142627
Received 29 May 2025; Received in revised form 5 July 2025; Accepted 7 July 2025
Available online 9 July 2025

U-wrapping can also provide a shear strength increase to a beam where shear forces are highest, and despite not fully constraining the slips in the jacketed (or wrapped) area of the CFRP-to-substrate interface, it may provide better constraints than increasing only the CFRP width. To improve the stress transfer between the CFRP composite and the substrate, researchers have proposed the additional use of CFRP spike anchors. This requires a series of drilling holes to be made in the substrate along the CFRP-to-substrate joint. However, the number of CFRP spike anchors or the distance between them is a subject that is not fully understood. Nevertheless, since CFRP composites have no shear strength, this type of anchorage may not be strong enough, and the CFRP rupture of the CFRP-to-substrate joint may occur. In any of these three cases, increasing the CFRP width, U-jacket (or wrap), and CFRP spike anchors are all CFRP anchorages to be used preferably with CFRP sheets rather than CFRP laminates or strips and can also be used as an end or a loaded anchorage.

The fourth and most prominent bonding technique of this first group of anchorages is the CREatE technique, which aims to embed both ends of the CFRP composite into the substrate's core. Both CFRP ends are then bonded, and in the case of a beam, the CFRP embedded length will be subjected to a compression stress developed by a strut inside the beam that increases with the bending loads. This compression stress is beneficial for the bond performance of the CFRP-to-concrete joint, avoiding premature debonding [9–11]. However, unlike the other three CFRP anchorages, the CREatE technique is easier to implement with CFRP laminates or strips (or stainless steel) instead of CFRP sheets. Since drilling holes is required, it is more suitable for concrete, timber or clay brick rather than steel structures.

From the second group of anchorages (see Fig. 1b), the transversely compressed steel anchorages are probably the most popular among researchers, e.g. [12–17]. The aim of transversely compressing the anchorage is to improve the bond between the CFRP and the substrate, which is achieved by enhancing the local bond behaviour between the adherends. For that to happen successfully, the compression stress, the anchorage length, and the friction angle of the interface are three crucial aspects for the high performance of this anchorage type. However, the increase in the anchorage length makes the increase in the compression stress more difficult due to the increase in the contact area with the CFRP composite. Therefore, by pre-treating the surface of both adherends, the internal friction angle of the CFRP-to-substrate interface may increase, and for this reason, it is the most critical aspect of the three previously mentioned parameters. It should also be noted that applying too high a compression stress may lead to the rupture of the carbon fibres of the CFRP composite, which damages and may compromise the final bond performance of the CFRP-to-substrate joint [18–20]. However, if a low-pressure magnitude is imposed on the transversely compressed anchorage, the CFRP composite may slip from inside the anchorage, making it useless. Although drilling holes is needed to fix the anchorage to the substrate through steel or chemical fasteners, this anchorage type has a wider application than any other anchorage, i.e., it can be used on any structural material. Other solutions can be found in the literature such as the use of π-shaped metallic anchorages [21–23],

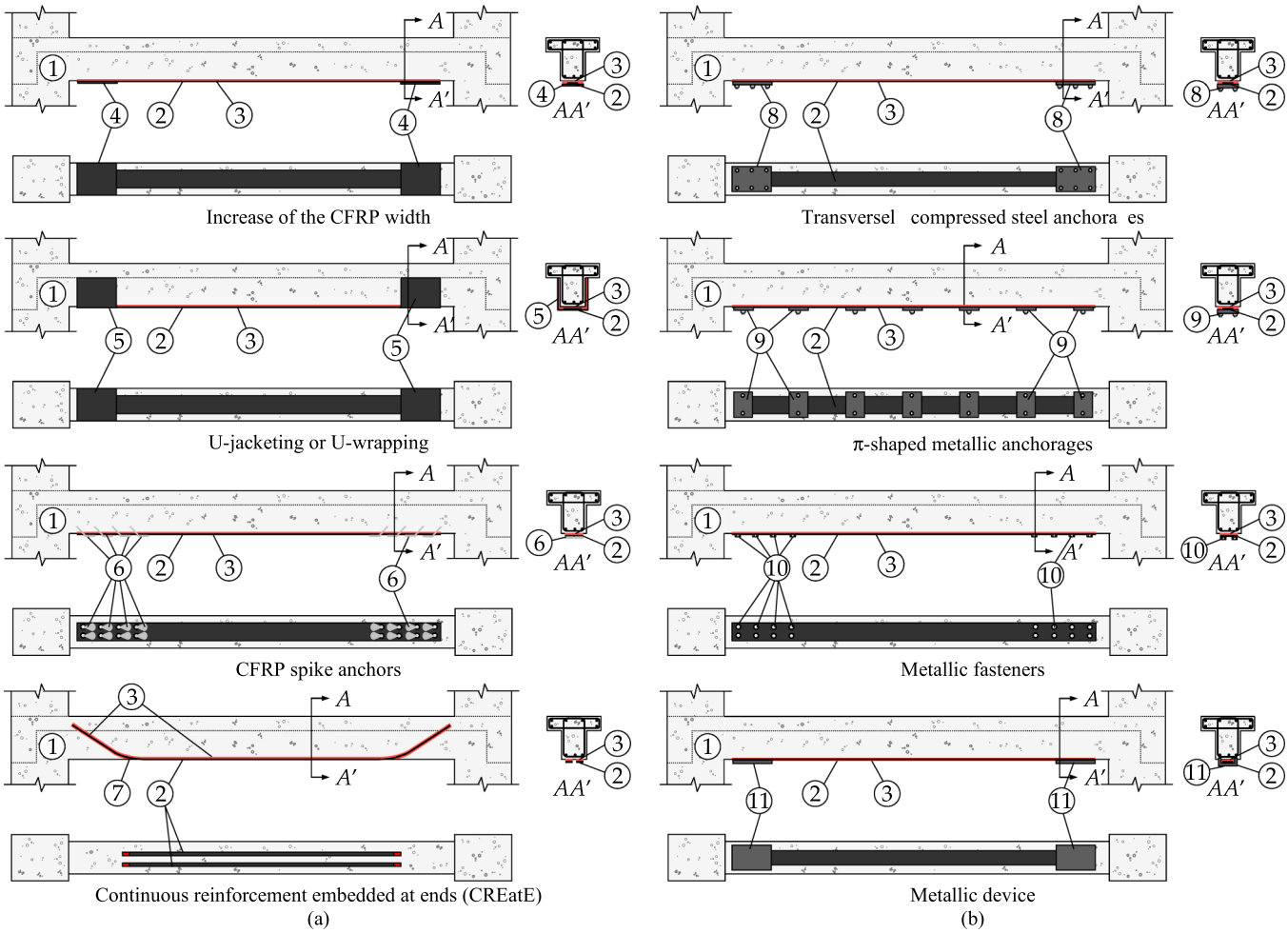

Fig. 1. Examples of mechanical anchorages: (a) CFRP anchorage group; and (b) Metallic anchorage group. Key: 1 – Reinforced concrete beam; 2 – FRP composite; 3 – Adhesive; 4 – Wider CFRP anchorage; 5 – CFRP U-jacketing or U-wrapping; 6 – CFRP spike anchors; 7 – Transition curve; 8 – Transversely compressed steel anchorage; 9 – π-shaped metallic anchorages; 10 – Metallic fasteners; 11 – Metallic device.

metallic fasteners (e.g., screws with or without a washer) or a metallic device that can fix the CFRP ends [24,25]. The use of metallic fasteners induces shear forces into the CFRP composite, leading to shear rupture, which makes them useless as an anchorage. Fixing the ends of the CFRP composite to a metallic device and installing it into a superficial layer of the substrate through metallic fasteners may be laborious. However, despite being tested in limited works [20], to the best of the author's knowledge, this technique still needs further research to confirm its effectiveness or lack of.

Due to the variety of anchorages and possible combinations, a full understanding is quite hard to achieve. Therefore, the wider application of any of these anchored FRP-to-substrate bonded joints is limited due to the persisting lack of knowledge of the bond performance, whether in an isolated or combined configuration, i.e., using an anchorage or combining different anchorages. Additionally, no general and simple analytical model has been developed yet that can mitigate that lack and allow its worldwide use by engineers or practitioners with confidence in the prediction and design of FRP-to-substrate joints with or without an additional mechanical anchorage regardless of its type and/or installation place throughout the bonded length of the joint. For these reasons, an analytical approach able to deal with end and/or loaded anchorages, as well as other anchorages placed somewhere at the centre of the FRP-to-substrate joints, is introduced in this work. The generalised analytical model (GAM) can be used regardless of the anchorage type, whose modelling is made by axial springs with a linear or nonlinear load-displacement (or strain-displacement) curve. The full load-slip curves of the anchored FRP-to-substrate joints are obtained, allowing the determination of the debonding load and the maximum load transmitted to the FRP composite. Although the GAM can be used with brittle or ductile adhesives, it is more suitable for the former since it is based on an exponential bond-slip relationship that can better reproduce the performance of an FRP composite bonded to a substrate with a brittle adhesive. However, with less accuracy, the same exponential bond-slip relationship was used in other studies [26,27] to represent the characteristic trapezoidal bond-slip relationship experimentally observed in FRP-to-substrate joints bonded with a ductile adhesive [5,28–30].

A total of 52 generated cases are studied with the GAM and the results are compared with those obtained from the use of a commercial package based on the finite element method (FEM). The results allowed us to validate the GAM due to the relatively low number of Integral Absolute Errors (IAE) found. Despite the scarcity in the literature, a series of experimental data collected from the literature [31–33] was simulated with the GAM, and there is good accuracy. Practical applications are shown at the end.

2. Description of the generalised analytical model

This section introduces the GAM, with its initial assumptions, situations that can be analytically simulated and derivation of the closed-form solutions that define the model and allow us to determine and characterise the complete debonding process of the FRP-to-substrate joints with or without anchorages.

2.1. Assumptions

Before starting the derivation of the model, we first need to establish the assumptions on which the GAM is based. The following derivations, which will allow us to obtain the closed-form solutions presented in subsection 2.3, are based on the main assumptions enumerated below:

(i) the Poisson's coefficient is not considered, and for this reason, the thicknesses of the adherends (FRP and substrate) do not change along the complete debonding process of the joints;
(ii) linear and elastic constitutive behaviours of the adherends are assumed. However, in the case of adherends with an elastic-plastic behaviour, yielding can be considered since the strains developed in the adherends can be controlled. This way, the GAM can predict the point where yielding of the substrate initiates or the rupture of the FRP composite, which defines the failure mode of the adhesively bonded joint. However, since the stiffness of the substrate is usually much higher than that of the FRP composite, the yielding of the substrate will most probably never occur;
(iii) along with the debonding process, the normal bond stresses (i.e., peeling stresses) can be ignored since the joints will not bend. Therefore, the normal bond stresses will have a low magnitude that can be ignored since they will have a low influence on the shear bond stresses, as suggested in the literature [19,34–37]. Consequently, only the deformations consistent with fracture mode II are considered;
(iv) the shear bond stresses developed across the width of the FRP composite are distributed evenly;
(v) the different anchorages and their load-displacement behaviours are modelled by a spring with linear or nonlinear behaviour, resulting in the cases shown in Fig. 2a. Moreover, if the stiffness of the springs is negligible (i.e., the stiffness of the spring on the left-hand side $k_0(s) \to 0$ and the stiffness of the spring on the right-hand side $k_L(s) \to 0$ as shown in Fig. 2a), then the common FRP-to-substrate joint shown in Fig. 2b is obtained. However, if only the stiffness of the loaded anchorage is negligible (i.e., $k_0(s) \neq 0$ and $k_L(s) \to 0$), then the configuration of the FRP-to-substrate shown in Fig. 2c is obtained, where no spring is shown on the right-hand side of this figure. On the other hand, if it is only the stiffness of the end anchorage that is negligible (i.e., $k_0(s) \to 0$ and $k_L(s) \neq 0$), then the configuration of the adhesively bonded joint can be represented by Fig. 2d;
(vi) the adhesive used to bond the FRP onto the substrate, as well as the substrate-to-FRP and adhesive-to-FRP interfaces, are all replaced by a non-thickness cohesive zone model (CZM). This CZM model correlates the interfacial slips (s) with the shear bond stresses (τ_b), which is usually called the bond-slip relationship of the adhesively bonded joint [38–44]. In the present case, the exponential bond-slip relationship originally proposed by Dai et al. [3] is used to approximate the local bond behaviour of the bonded joints. As well as the good accuracy of this exponential bond-slip relationship to represent the local bond behaviour of several adhesively bonded joints, it is easy to find a derivative or to integrate, which also makes it a good function to use when determining the analytical debonding of FRP-to-substrate joints. This exponential function is defined according to [3]:

$$\tau_b = B \cdot G_F \cdot \left(e^{-B \cdot s} - e^{-2B \cdot s}\right) \tag{1}$$

where B is the stiffness index of the interface, and G_F is the mode II fracture energy. To avoid unnecessarily increasing the text, more details on the derivation of this bond-slip relationship can be found in the work carried out by Dai et al. [3].

2.2. Possible situations covered by the GAM

From the assumptions previously made, the proposed analytical model can cover a series of different cases that are identified below. Despite the fact it is not possible to show all the anchorages documented in the literature in Fig. 3, e.g., CFRP spike anchors [31,45–48], mixed adhesives [27,48,49], Continuous Reinforcement Embedded at Ends (CREatE) [9–11], Externally Bonded Reinforcement In Grooves (EBRIG) or On Grooves (EBROG) [50–54], among others, and possible combinations between them, the proposed analytical model can deal with all of them once the load-slip behaviour of each anchorage is known. Thus, the situations shown in Fig. 3 consider the particular use of a transversely compressed anchorage and/or a CFRP U-wrap anchorage and correlate them with the theoretical model from which the closed-form solutions can be analytically derived. Although less common in the

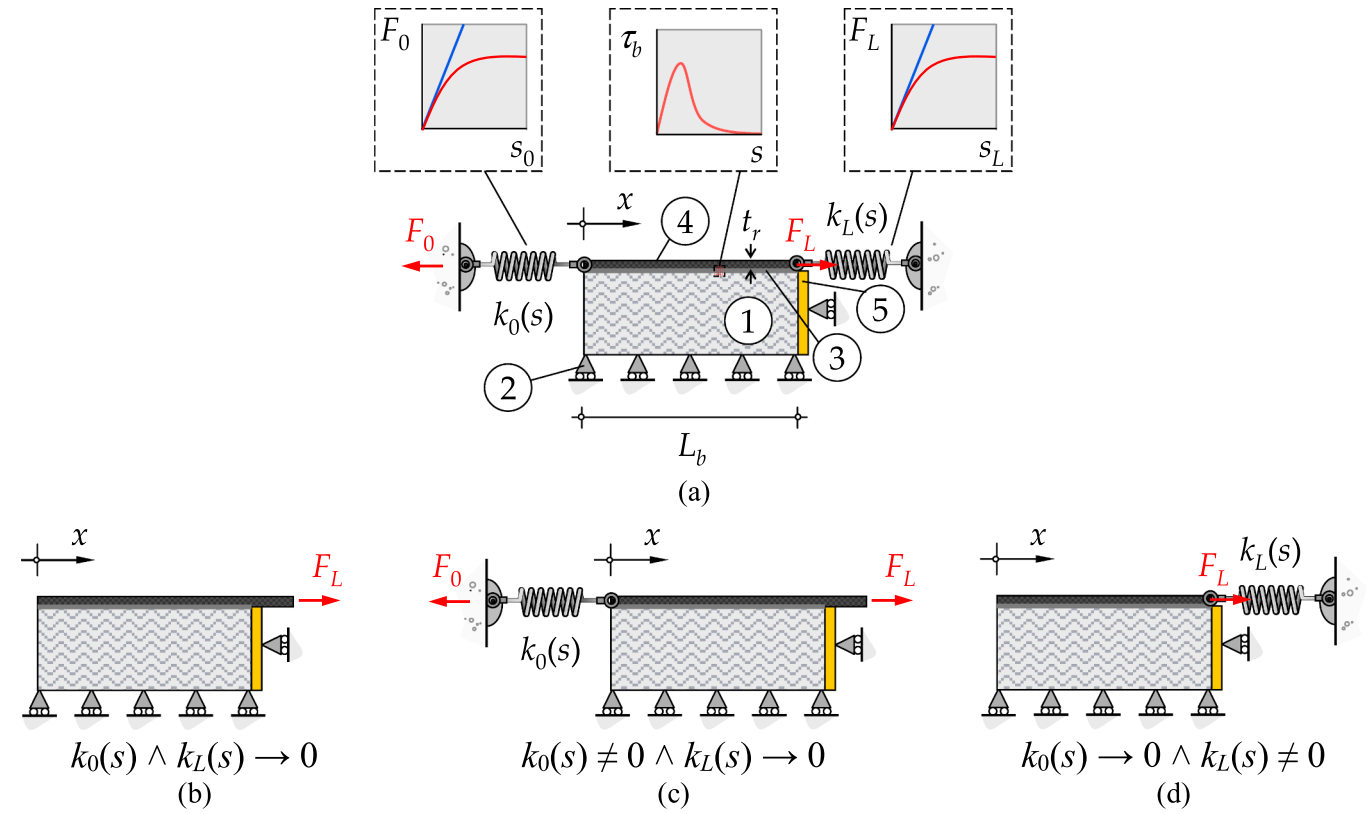

Fig. 2. Situations covered by the analytical model: (a) general case with an end and a loaded anchorage simulated by two springs with stiffnesses $k_0(s)$ and $k_L(s)$, respectively; (b) with no springs whose stiffnesses tend to a zero value; (c) with an end anchorage simulated by a spring with stiffness $k_0(s)$; and (d) with a loaded anchorage simulated by a spring with stiffness $k_L(s)$. Key: 1 – Substrate; 2 – Roller support; 3 – Adhesive; 4 – FRP strip; 5 – Steel reaction plate.

literature, glass (G) or basalt (B) FRP composites bonded to concrete, timber, steel or clay brick substrates can also be considered in the GAM. However, it should be noted that the bond-slip relationship between both dissimilar materials can always be approximated by Eq. (1).

Furthermore, the GAM is not limited to the situations shown in Fig. 3, i.e., to the assumption of an end and/or loaded anchorages. Another case of an anchorage placed somewhere in the centre of the FRP-to-substrate bonded joint can also be considered (see Fig. 4). However, in this case, the analytical model should follow certain steps so that the debonding process of those mechanically anchored joints can be determined.

Depending on what is initially known, two approaches can be followed. The first and more laborious approach is shown in Fig. 4a.i–.iv (or Fig. 3b.i–.iv), and the rationale behind it is as follows: once the load-slip (F_a-s_a) curve of the anchorage is known (Figs. 4a.i or 4b.i), the GAM can be used by considering an adhesively bonded joint with a loaded end anchorage (see Figs. 4a.iii or 4b.iii) that is analytically simulated by a spring with the same F_a-s_a curve (see Figs. 4a.ii or 4b.ii). Then, from the resultant load-slip curve, the GAM can be used once again by defining a new spring as an end anchorage with a load-slip behaviour F_0-s_0, which is the same F_0-s_0 curve obtained from the previous step (see Figs. 4a.iv or 4b.iv).

Alternatively, the problem is less laborious if the load-slip curve (F_0-s_0 curve) is already known (see Figs. 4a.iii or 4b.iii). In this case, the GAM is used only once, and the FRP-to-substrate joint with an end anchorage is solved by considering the problem defined in Figs. 4a.iv or 4a.iv.

2.3. Closed-form solution for the general debonding process

From the equilibrium of a finite length dx of a generalised FRP-to-substrate joint, i.e., with or without anchorages, the governing equation that describes the debonding process of the joints shown in Fig. 3 follows the same well-known governing equation of an FRP-to-substrate joint with no mechanical anchorages, e.g. [2,55–59], i.e.

$$\frac{d^2s}{dx^2} - \lambda \cdot \tau_b(s) = 0 \tag{2}$$

where x represents the axis parallel to the total bonded length of the joint (see Fig. 3) and

$$\lambda = \frac{1}{E_r \cdot t_r} + \frac{b_r}{E_s \cdot A_s} \tag{3}$$

where E_r and E_s are the elastic moduli of the FRP composite and substrate, respectively; t_r and b_r are the thickness and width of the FRP composite, respectively; and A_s is the cross-sectional area of the substrate ($t_s \times b_s$ – thickness × width).

Introducing Eq. (1) into Eq. (2), the governing equation of the debonding process is defined according to:

$$\frac{d^2s}{dx^2} - \lambda \cdot B \cdot G_F \cdot \left(e^{-B \cdot s} - e^{-2B \cdot s}\right) = 0 \tag{4}$$

The solution of Eq. (4) can be found by bearing in mind that

$$\frac{d^2s}{dx^2} = \frac{d}{dx}\left(\frac{ds}{dx}\right) = \frac{d}{ds}\left(\frac{ds}{dx}\right)\frac{ds}{dx} = \frac{1}{2}\frac{d}{ds}\left(\frac{ds}{dx}\right)^2 \tag{5}$$

So, introducing Eq. (5) in Eq. (13) yields

$$\left(\frac{ds}{dx}\right)^2 = \int 2\lambda \cdot B \cdot G_F \cdot \left(e^{-B \cdot s} - e^{-2B \cdot s}\right) ds \tag{6}$$

Considering that

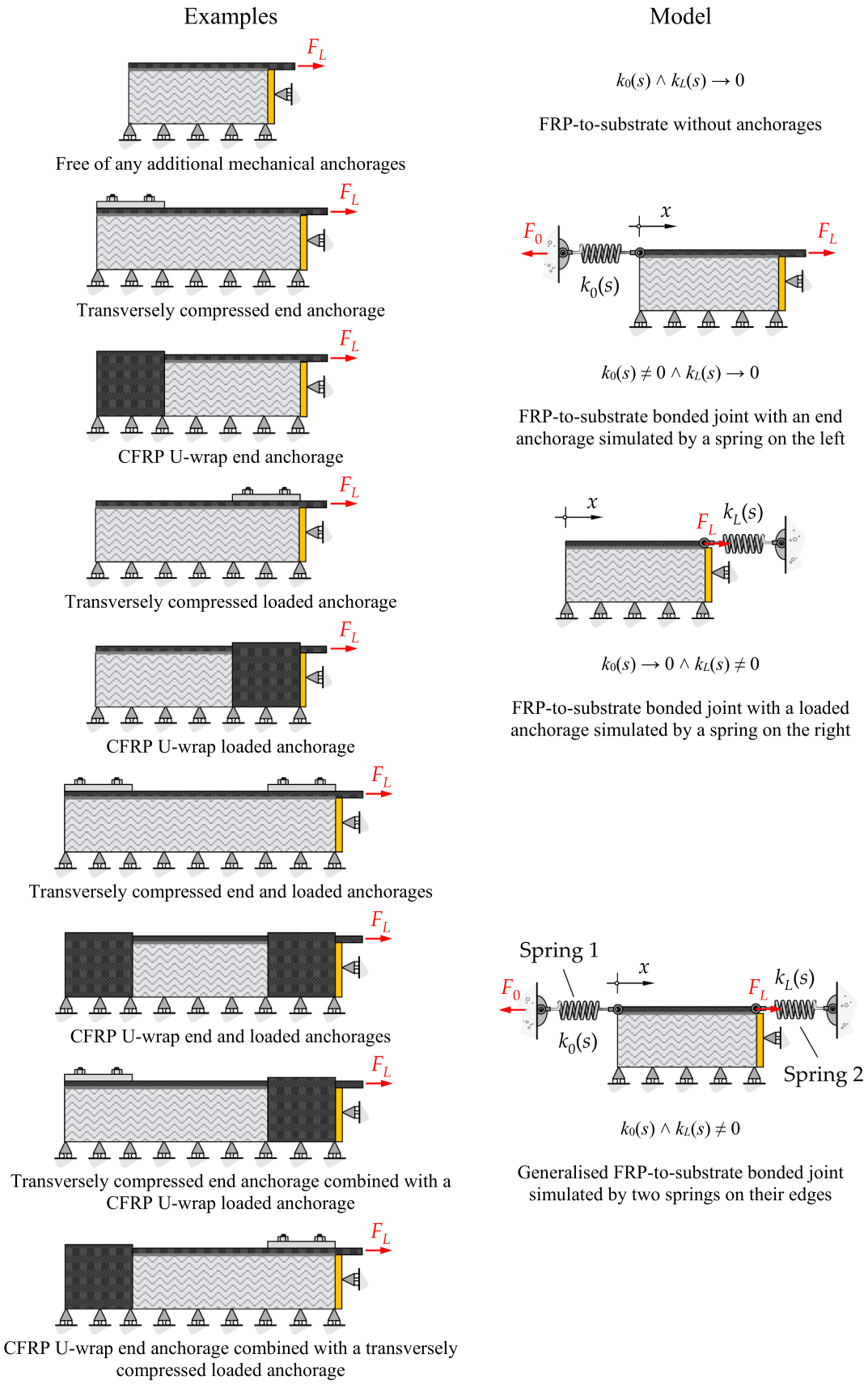

Fig. 3. Some examples covered by the GAM.

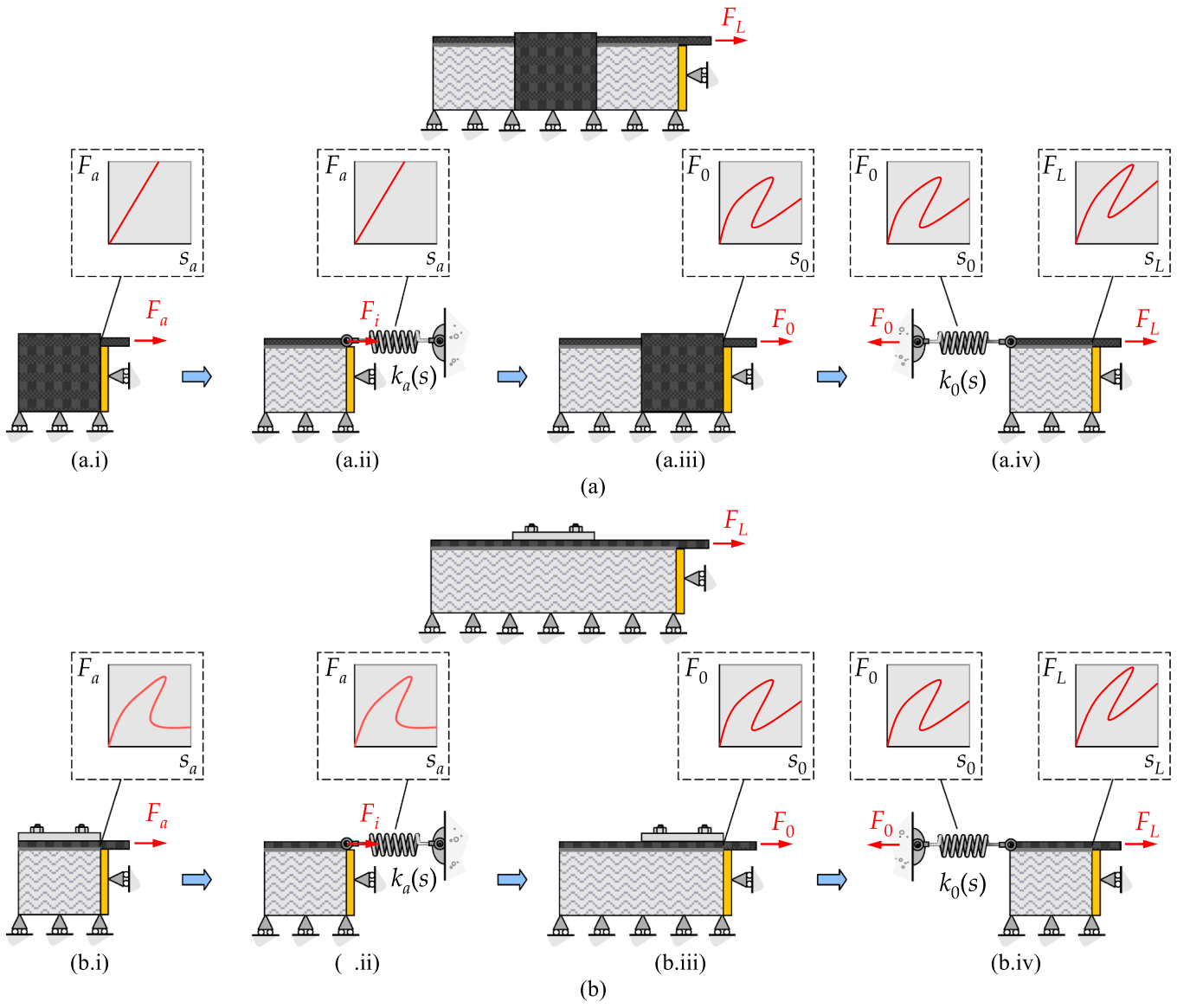

Fig. 4. Strategy to obtain the debonding process of an FRP-to-substrate joint with an anchorage installed at the centre of the total bonded length with a: (a) linear behaviour; and (b) nonlinear behaviour.

$$2B\cdot\left(e^{-B\cdot s}-e^{-2B\cdot s}\right)=\frac{d}{ds}\left(1-e^{-B\cdot s}\right)^2 \tag{7}$$

Eq. (6) can be rewritten as follows

$$\left(\frac{ds}{dx}\right)^2=\int 2\lambda\cdot G_F\cdot\frac{d}{ds}\left(1-e^{-B\cdot s}\right)^2 ds \tag{8}$$

which, when integrated, leads to:

$$\frac{ds}{dx}=\sqrt{2\lambda\cdot G_F\cdot\left(1-e^{-B\cdot s}\right)^2+C_1} \tag{9}$$

where C_1 is a constant of integration that can be found from the strains developed at the FRP composite unloaded end, i.e., ε_{r0}. To find the value of C_1, it should be noted that the strains in the FRP composite are defined according to [60–62]:

$$\varepsilon_r=\frac{1}{1+r}\cdot\frac{ds}{dx} \tag{10}$$

where r is the ratio between the axial stiffness of the FRP composite and the axial stiffness of the substrate, respectively. Introducing Eq. (9) in Eq. (10) and writing it at $x=0$, i.e. at the FRP unloaded end, yields:

$$\varepsilon_{r0}=\frac{1}{1+r}\cdot\sqrt{2\lambda\cdot G_F\cdot\left(1-e^{-B\cdot s_0}\right)^2+C_1} \tag{11}$$

where s_0 is the slip at $x=0$. Isolating C_1 in Eq. (11) leads to:

$$C_1=\varepsilon_{r0}{}^2\cdot(1+r)^2-D^2\cdot\left(1-e^{-B\cdot s_0}\right)^2 \tag{12}$$

where D is a positive constant defined by

$$D=\sqrt{2\lambda\cdot G_F}. \tag{13}$$

To find the slips developed throughout the bonded length, Eq. (9) is rewritten as follows

$$\frac{ds}{\sqrt{\left(1-e^{-B\cdot s}\right)^2+\left(\frac{\sqrt{|C_1|}}{D}\right)^2}}=D dx \tag{14}$$

Integrating Eq. (14) gives

$$\frac{D\cdot \text{ar sinh}\left(\frac{\left(D^2+C_1\right)\cdot e^{B\cdot s}-D^2}{\sqrt{|C_1|}\cdot D}\right)}{B\cdot\sqrt{|D^2+C_1|}}=D\cdot x+C_2 \tag{15}$$

where C_2 is another constant of integration. This constant can be found from the boundary condition at $x = 0$. Thus, at this point, the slips are $s = s_0$. Isolating the term corresponding to the interfacial slips (s) in Eq. (15), these are analytically defined along the bonded length according to

$$s(x)=\frac{1}{B}\cdot\ln\left[\frac{D^2+\sqrt{|C_1|}\cdot D\cdot\sinh\left(\frac{B\cdot(D\cdot x+C_2)\cdot\sqrt{|D^2+C_1|}}{D}\right)}{|D^2+C_1|}\right] \tag{16}$$

where

$$C_2=\frac{D\cdot \text{ar sinh}\left(\frac{\left(D^2+C_1\right)\cdot e^{B\cdot s_0}-D^2}{\sqrt{|C_1|}\cdot D}\right)}{B\cdot\sqrt{|D^2+C_1|}} \tag{17}$$

The strains developed in the FRP composite can be defined by introducing the first derivative of Eq. (16) with respect to x into Eq. (10)

$$\varepsilon_r(x)=\frac{1}{1+r}\cdot\frac{\sqrt{|C_1+D^2|}\cdot\cosh\left(\frac{B\cdot(D\cdot x+C_2)\cdot\sqrt{|C_1+D^2|}}{D}\right)}{\sinh\left(\frac{B\cdot(D\cdot x+C_2)\cdot\sqrt{|C_1+D^2|}}{D}\right)+\frac{D}{\sqrt{|C_1|}}} \tag{18}$$

The bond stresses developed throughout the bonded length can be defined by introducing Eq. (16) into Eq. (1), leading to

$$\tau_b(x)=B\cdot G_F\cdot\frac{\frac{D}{\sqrt{|C_1|}}+\frac{\sqrt{|C_1|}}{D}}{\frac{D}{\sqrt{|C_1|}}+\sinh\left(B\cdot(D\cdot x+C_2)\cdot\sqrt{\left|1+\frac{C_1}{D^2}\right|}\right)}\times\left(1-\frac{\frac{D}{\sqrt{|C_1|}}+\frac{\sqrt{|C_1|}}{D}}{\frac{D}{\sqrt{|C_1|}}+\sinh\left(B\cdot(D\cdot x+C_2)\cdot\sqrt{\left|1+\frac{C_1}{D^2}\right|}\right)}\right) \tag{19}$$

The strains developed in the substrate can also be found by using the expression derived by the authors in other works, e.g. [60–62]

$$\varepsilon_s=-\frac{1}{1+\frac{1}{r}}\cdot\frac{ds}{dx} \tag{20}$$

Thus, introducing the first derivative of Eq. (16) with respect to x in Eq. (20), it gives

$$\varepsilon_s(x)=-\frac{1}{1+\frac{1}{r}}\cdot\frac{\sqrt{|C_1+D^2|}\cdot\cosh\left(\frac{B\cdot(D\cdot x+C_2)\cdot\sqrt{|C_1+D^2|}}{D}\right)}{\sinh\left(\frac{B\cdot(D\cdot x+C_2)\cdot\sqrt{|C_1+D^2|}}{D}\right)+\frac{D}{\sqrt{|C_1|}}} \tag{21}$$

From Eqs. (16) and (18), the load-slip (or strain-slip) curve of the spring on the left-hand side is considered regardless of its linearity (or nonlinearity). Moreover, this load-slip (F_0-s_0) curve controls the GAM. The slips at $x = L_b$ obtained from Eq. (16) and the displacements of the spring on the right-hand side of the generalised FRP-to-substrate joint are the same, i.e., at that point, it is under a parallel configuration. Therefore, the loads transmitted to the generalised FRP-to-substrate bonded joint correspond to the sum of the loads determined from Eq. (18) with the loads from the load-displacement curve of the spring on the right-hand side of the generalised FRP-to-substrate joint, i.e.:

$$F_L=\frac{E_r\cdot A_r}{1+r}\cdot\frac{\sqrt{|C_1+D^2|}\cdot\cosh\left(\frac{B\cdot(D\cdot L_b+C_2)\cdot\sqrt{|C_1+D^2|}}{D}\right)}{\sinh\left(\frac{B\cdot(D\cdot L_b+C_2)\cdot\sqrt{|C_1+D^2|}}{D}\right)+\frac{D}{\sqrt{|C_1|}}}+F_{\text{spring},2}(s_L) \tag{22}$$

where $F_{\text{spring},2}(s_L)$ is the load in the right-hand spring when the slip of the generalised FRP-to-substrate bonded joint at $x = L_b$ is s_L.

3. Case studies

3.1. Geometry, dimension and mechanical properties of the materials

For the cases under study in this work, CFRP-to-concrete interfaces were selected. Since the exponential bond-slip relationship defined in Eq. (1) could define the local bond behaviour between adherends, other joint types could be assumed, e.g., CFRP composites externally bonded to steel, timber, clay bricks, etc. Although Eq. (1) is associated with adhesively bonded structures where a brittle adhesive was used to bond the adherends, ductile adhesives can also be used, even though slightly less accurately, as documented in the literature [26,27]. Nevertheless, the lack of accuracy is not great, and the debonding process of such joints can be estimated with a fair degree of accuracy.

The unidirectional CFRP composite used and tested by Carvalho et al. [63] was considered. Its average mechanical properties in the direction of the fibres were obtained from the uniaxial tension tests of five specimens, leading to the following results: elastic modulus of 159 GPa, tensile strength of 1565 MPa, and a rupture strain approximately equal to 1.0 %. The CFRP strip has a thickness of 1.4 mm and a width of 10 mm, and it was supplied by a local S&P manufacturer.

The S&P 220 resin [64] was used to bond the CFRP strip onto the reinforced concrete block. This adhesive is a bi-component resin, i.e., with an epoxy resin and a hardener, which were mixed in the proportion of 4:1 (resin:hardener) as recommended by the manufacturer [64]. To obtain the mechanical properties of the resin, Carvalho et al. [63] conducted three-point bending tests on three resin specimens measuring 160 × 40 × 40 mm. From the mechanical characterisation tests of the resin under tension, an elastic modulus of 0.79 GPa and a strain of 3.65 % were obtained. The resin showed a stress-strain relationship with a brittle failure rather than a ductile one.

The same CFRP strip and adhesive were used by Borba [65], who conducted a series of experimental single-lap shear tests with CFRP bonded to a reinforced concrete block. In her study [65], the reinforced concrete substrate had a cross-sectional area of 300 × 300 mm (width × thickness), was 650 mm long and was built with 8 longitudinal ribbed steel rebars with a nominal diameter of 10 mm and 7 steel stirrups with a diameter of 6 mm placed 100 mm apart. The average mechanical properties of the concrete were determined from the uniaxial compression test of three 150 mm cubes. The mean compression stress obtained from these tests was $f_{cm,cub} = 22.74$ MPa, with, according to Eurocode 2 [66], an equivalent value in cylinders of $f_{cm} = 18.19$ MPa, i.e., with $f_{cm} = 0.8\ f_{cm,cub}$. The mean tensile stress and the elastic modulus of the concrete were also estimated through the formulae in Eurocode 2 [66], leading to $f_{cm} = 1.76$ MPa and $E_c = 26.33$ GPa, respectively.

The contact between the CFRP composite and the concrete block was experimentally calibrated with the same exponential bond-slip relationship defined in Eq. (1). Thus, Borba [65] determined that the index stiffness of the CFRP-to-concrete interface was $B = 11.552\ \text{mm}^{-1}$, a maximum shear bond stress of $\tau_{b,\max} = 10.19$ MPa, and a fracture energy of $G_F = 1.764$ N/mm. However, Borba [65] did not perform any tests with an additional anchorage. Therefore, the results obtained from the

work carried out by Codina et al. [32] are considered since they tested some CFRP-to-concrete bonded joints with a transversely compressed anchorage. Although the CFRP strips used by Codina et al. [32] were 50 mm wide, they were made by the same S&P manufacturer and have similar mechanical properties. The results that allow us to define the bond-slip relationship of such anchored bonded joints are briefly discussed later in Section 3.3.

Since the bonded length has a relevant impact on the bond performance of adhesively bonded structures, two bonded lengths are also considered. One bonded length is shorter than the effective bond length, i.e. the length beyond which no further loads can be transmitted to the FRP composite [67–70], and another bonded length is longer than the effective bond length. From the study carried out by Borba [65], an effective bond length of the CFRP-to-concrete interface is approximately 185 mm. Thus, a bonded length of 50 mm and another of 250 mm were considered. Two anchorage lengths were also considered since they also have an important influence on the bond performance of the anchored FRP-to-substrate joints [37,71,72]. In this case, the definition of the load-displacement curves of the anchorages was estimated through a simple numerical process described in subsection 3.3.

3.2. Description of the generated cases

To highlight the wide applicability of the GAM, a series of generated cases is considered. Hence, the generated cases cover the influences of the: (i) the bonded length (L_b); (ii) the load-displacement behaviour of the spring, i.e., with a linear or nonlinear behaviour; (iii) regarding the previous item, the stiffness of the spring with a linear load-displacement behaviour, i.e., with 0 N/mm (i.e., no spring), 10,000 N/mm, and 150,000 N/mm; (iv) two nonlinear behaviours of the springs, i.e., obtained from short and long anchorage lengths (L_a); and (v) the combination of the previous springs considered in the three previous items. As a result, a total of 52 generated cases were analysed. To facilitate the identification of each one, Table 1 summarises all of them.

To identify the generated cases adopted all the previously mentioned aspects were considered in the following order: adherends, bonded length, stiffness of spring 1, and stiffness of spring 2. In the case of a nonlinear spring, the term "nonlinear" is used instead of the value of the stiffness of the spring. Since two nonlinear springs were considered, they are distinguished by adding the numbers 1 and 2 after the term nonlinear. Hence, the case of the spring with the "nonlinear 1" behaviour represents the load-displacement of a bonded joint with a short transversely compressed anchorage, whereas "nonlinear 2" corresponds to the load-displacement of a long transversely compressed anchorage. The definition of these two curves is explained in the next subsection.

Therefore, e.g., specimen CS50-K0_nonlinear1-KL_10000 aims to identify a generalised CFRP-to-substrate bonded joint (CS) with a bonded length of 50 mm with a transversely compressed short end anchorage and a loaded anchorage with a linear behaviour and stiffness of 10,000 N/mm.

3.3. Definition of the load-displacement of the springs

For the definition of the load-displacement curves of the springs with nonlinear behaviour, the following relationship is used:

$$\tau_b = E_r \cdot t_r \cdot \frac{d\varepsilon_r}{ds} \cdot \frac{ds}{dx} \tag{23}$$

Introducing Eq. (10) into Eq. (23) yields

$$\tau_b = (1+r) \cdot E_r \cdot t_r \cdot \frac{d\varepsilon_r}{ds} \cdot \varepsilon_r \tag{24}$$

The approximation of Eq. (24) is

$$\tau_{b,i+1} = (1+r) \cdot E_r \cdot t_r \cdot \frac{\varepsilon_{r,i+1} - \varepsilon_{r,i}}{s_{i+1} - s_i} \cdot \varepsilon_{r,i+1} \tag{25}$$

Table 1
ID of all generated cases under study.

ID	Bonded length, L_b (mm)	Stiffness of the end anchorage, k_0 (N/mm)	Stiffness of the loaded anchorage, k_L (N/mm)
CS50-K0_0-KL_0	50	0	0
CS50-K0_10000-KL_0		10,000	0
CS50-K0_150000-KL_0		150,000	0
CS50-K0_inf-KL_0		∞	0
CS50-K0_nonlinear1-KL_0		Nonlinear 1	0
CS50-K0_nonlinear2-KL_0		Nonlinear 2	0
CS50-K0_0-KL_10000		0	10,000
CS50-K0_0-KL_150000		0	150,000
CS50-K0_0-KL_nonlinear1		0	Nonlinear 1
CS50-K0_0-KL_nonlinear2		0	Nonlinear 2
CS50-K0_10000-KL_10000		10,000	10,000
CS50-K0_10000-KL_150000		10,000	150,000
CS50-K0_150000-KL_10000		150,000	10,000
CS50-K0_150000-KL_150000		150,000	150,000
CS50-K0_10000-KL_nonlinear1		10,000	Nonlinear 1
CS50-K0_10000-KL_nonlinear2		10,000	Nonlinear 2
CS50-K0_150000-KL_nonlinear1		150,000	Nonlinear 1
CS50-K0_150000-KL_nonlinear2		150,000	Nonlinear 2
CS50-K0_nonlinear1-KL_10000		Nonlinear 1	10,000
CS50-K0_nonlinear1-KL_150000		Nonlinear 1	150,000
CS50-K0_nonlinear2-KL_10000		Nonlinear 2	10,000
CS50-K0_nonlinear2-KL_150000		Nonlinear 2	150,000
CS50-K0_nonlinear1-KL_nonlinear1		Nonlinear 1	Nonlinear 1
CS50-K0_nonlinear1-KL_nonlinear2		Nonlinear 1	Nonlinear 2
CS50-K0_nonlinear2-KL_nonlinear1		Nonlinear 2	Nonlinear 1
CS50-K0_nonlinear2-KL_nonlinear2		Nonlinear 2	Nonlinear 2
CS250-K0_0-KL_0	250	0	0
CS250-K0_10000-KL_0		10,000	0
CS250-K0_150000-KL_0		150,000	0
CS250-K0_inf-KL_0		∞	0
CS250-K0_nonlinear1-KL_0		Nonlinear 1	0
CS250-K0_nonlinear2-KL_0		Nonlinear 2	0

(continued on next page)

Table 1 (*continued*)

ID	Bonded length, L_b (mm)	Stiffness of the end anchorage, k_0 (N/mm)	Stiffness of the loaded anchorage, k_L (N/mm)
CS250-K0_0-KL_10000		0	10,000
CS250-K0_0-KL_150000		0	150,000
CS250-K0_0-KL_nonlinear1		0	Nonlinear 1
CS250-K0_0-KL_nonlinear2		0	Nonlinear 2
CS250-K0_10000-KL_10000		10,000	10,000
CS250-K0_10000-KL_150000		10,000	150,000
CS250-K0_150000-KL_10000		150,000	10,000
CS250-K0_150000-KL_150000		150,000	150,000
CS250-K0_10000-KL_nonlinear1		10,000	Nonlinear 1
CS250-K0_10000-KL_nonlinear2		10,000	Nonlinear 2
CS250-K0_150000-KL_nonlinear1		150,000	Nonlinear 1
CS250-K0_150000-KL_nonlinear2		150,000	Nonlinear 2
CS250-K0_nonlinear1-KL_10000		Nonlinear 1	10,000
CS250-K0_nonlinear1-KL_150000		Nonlinear 1	150,000
CS250-K0_nonlinear2-KL_10000		Nonlinear 2	10,000
CS250-K0_nonlinear2-KL_150000		Nonlinear 2	150,000
CS250-K0_nonlinear1-KL_nonlinear1		Nonlinear 1	Nonlinear 1
CS250-K0_nonlinear1-KL_nonlinear2		Nonlinear 1	Nonlinear 2
CS250-K0_nonlinear2-KL_nonlinear1		Nonlinear 2	Nonlinear 1
CS250-K0_nonlinear2-KL_nonlinear2		Nonlinear 2	Nonlinear 2

where $\tau_{b,i+1}$ is the shear bond stress at point $i+1$ of the strain-slip relationship; $\varepsilon_{r,i+1}$ and $\varepsilon_{r,i}$ are the FRP strains at point $i+1$ and i of the strain-slip relationship, respectively; and s_{i+1} and s_i are the slips at point $i+1$ and i of the strain-slip relationship, respectively.

To obtain the load-slip (or strain-slip) of the FRP-to-substrate joint from the bond-slip relationship, Eq. (25) is solved regarding the term ε_{i+1}, i.e.:

$$\varepsilon_{r,i+1}{}^2 - \varepsilon_{r,i}\cdot\varepsilon_{r,i+1} - \frac{\tau_{b,i+1}\cdot(s_{i+1}-s_i)}{E_r\cdot t_r\cdot(1+r)} = 0 \tag{26}$$

The solution of the 2nd-order polynomial equation in (26) allows the determination of the strains of the FRP composite at s_{i+1} as follows:

$$\varepsilon_{r,i+1} = \frac{\varepsilon_{r,i}}{2} + \sqrt{\left(\frac{\varepsilon_{r,i}}{2}\right)^2 + \frac{\tau_{b,i+1}\cdot(s_{i+1}-s_i)}{E_r\cdot t_r\cdot(1+r)}} \tag{27}$$

Although Eq. (27) can be used regardless of the bond-slip relationship, it only gives the strain-slip (or load-slip) of an FRP-to-substrate bonded joint with a long-bonded length. For this reason, the load-slip of a short-bonded length is directly obtained from the bond-slip relationship by assuming that the bond stresses along the bonded length are constant, i.e.:

$$F = \tau_b\cdot A_r \tag{28}$$

To represent the local bond behaviour of the transversely compressed mechanical anchorage, the bond-slip relationship originally proposed by the authors [73] is used:

$$\tau_b(s) = \beta\cdot\left(\sigma_n\cdot\tan(\phi)+\tau_{b,\,\max\,0}\right)\cdot\left(1-e^{-b\cdot s}\right)\cdot\frac{\frac{\sigma_n\cdot\tan(\phi)}{\beta\cdot\left(\sigma_n\cdot\tan(\phi)+\tau_{b,\,\max\,0}\right)}+e^{-a\cdot(s-s_t)}}{1+e^{-a\cdot(s-s_t)}} \tag{29}$$

where β is a dimensionless parameter that ensures the maximum shear bond stress is reached and can be obtained by a simple trial and error process; a and b are two parameters to be calibrated with the experimental data; s_t is the slip that usually corresponds to the midpoint of the transition between the maximum ($\tau_{b,\max}$) and the frictional ($\tau_{b,f}$) stresses; σ_n is the compression stress (with positive signal) applied by the mechanical anchorage to the bonded joint; $\tau_{b,\max 0}$ is the shear bond stress of the bonded joint free of any external compressions; and ϕ is the friction angle of the interface.

In the present work, the parameters that define Eq. (29) are quantified as follows: $a = 13.241$, $b = 29.453$, $s_t = 0.356$ mm, $\beta = 1.035$, $\phi = 0.75$ rad, $\sigma_n = 4.88$ MPa and $\tau_{b,\max 0} = 8.43$ MPa. The parameters were obtained from the work carried out by Codina et al. [32], who studied the bond performance of CFRP-to-concrete joints and derived the corresponding bond-slip relationship from a teaching-learning-based optimisation (TLBO) algorithm. Since Codina et al. [32] used a 50 mm-wide strip of CFRP, the subsequent load-displacement curves of a short and long bonded joint with a transversely compressed anchorage, shown in Fig. 5, were adjusted to a 10 mm-wide CFRP strip, which is the same CFRP width used by Borba [65]. Both load-slip curves in Fig. 5 were obtained from the use of Eq. (27), which allowed us to estimate the load-displacement curves of CFRP-to-concrete bonded joints with a short and long anchorage length.

4. Simulation with the finite element method

Adhesively bonded structures have been numerically simulated by different FE software with success, e.g. [70,74–78]. However, since it has shown good results in modelling the debonding problem of FRP composites bonded to a substrate, e.g. [18,19,27,61,79], the FEM commercial ATENA package [80] was used to model the generated cases. Like other previous versions, the most recent version of the software allows us to model structures in a 2D and 3D environment. To significantly reduce the number of unknowns and nonlinear equations to be solved by the Newton-Raphson method, the 2D environment was used. In addition, the number of finite elements is reduced, decreasing

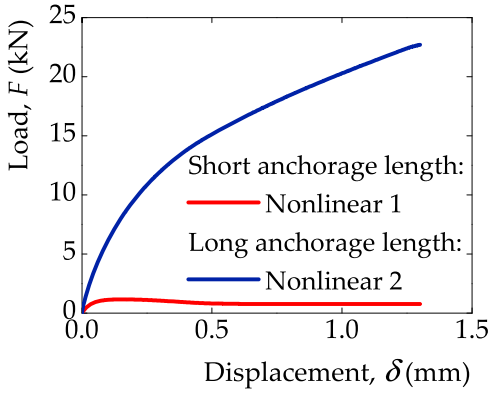

Fig. 5. Adopted load-displacement curves for the springs with a nonlinear behaviour.

the time required to process the models without losing precision during the simulations. Furthermore, this 2D environment is closer to the assumptions of the GAM.

The contact between the CFRP and the substrate is based on the Cohesive Zone Modelling (CZM). This CZM used in ATENA [80] couples fracture mode I with fracture mode II, i.e., in the case of the development of peeling stresses (normal bond stresses), the shear bond stresses are influenced according to the Mohr-Coulomb criterion. Hence, the friction angle of the interface has an important role in the correct simulation of the FRP-to-substrate debonding process since it significantly affects the bond performance of adhesively bonded structures when subjected to a mixed mode condition, i.e., mode I + II [18,19,37,81]. For instance, with a zero friction angle, the potential normal bond stresses developed throughout the interface of the joint will not influence the shear bond stresses, but an exaggerated value will meaningfully affect the shear bond stresses. For this reason, a correct value of the interfacial friction angle should be considered for the adhesively bonded structure.

Fig. 6 shows the numerical model with the shortest bonded length generated in ATENA [80] 2D environment. The materials, geometries and dimensions of the models were the same as those used by Borba [65] and already briefly described in Section 3. However, since the axial stiffness of the concrete substrate is too high when compared with the axial stiffness of the CFRP composite, the substrate was modelled as a rigid material with a thickness of 10 mm. This option allowed us to reduce the number of finite elements used for each model even more, especially in the models with the longest bonded lengths, i.e., 250 mm long. Consequently, the processing time for each 2D model was further reduced.

The loads were simulated by a regular monotonic displacement increment of 0.002 mm per step applied at the right-hand of the model. Four monitoring points were used to control the simulations. The first one controlled the displacements during the simulation and was placed exactly at point of the displacement increase. The other two monitoring points controlled the loads in the model, one placed at the same point as the previous monitoring point to assess the loads in spring 2 (on the right-hand side of the model), and another one placed on the left-hand side of the model to check the loads in spring 1. The fourth monitoring point was placed at the midpoint of the rigid substrate. The complete debonding of each model was reached regardless of the number of steps considered in each simulation.

Close to the contact between adherends, the meshes of the models were discretised with quadrilateral finite elements with smooth element shapes of 0.7–1.4 mm in the CFRP composite and the rigid substrate, respectively. Since two bonded lengths were considered (50 mm and 250 mm), the shortest model has the fewest number of finite elements (425 finite elements), whereas the longest model has 1929 finite elements. Consequently, in an Intel Core i7-7700HQ laptop computer at 2.80 GHz with 16 GB of 2400 MHz RAM, the simulations were carried out for a minimum of approximately 10 min (in the shortest models with the lowest number of finite elements), and 30 min (in the longest models with the highest number of finite elements).

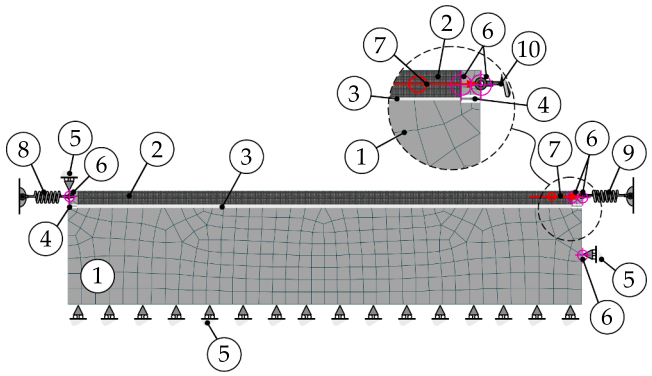

Key: 1 – Rigid substrate; 2 – CFRP composite; 3 – Interface element; 4 – Interface with no contact; 5 – Roller support; 6 – Monitoring point; 7 – Displacement increment point; 8 – End anchorage simulated by a spring with a linear or nonlinear behaviour (spring 1); 9 – Loaded anchorage simulated by a spring with a linear or nonlinear behaviour (spring 2).

Fig. 6. Mesh of the generated models with the shortest bonded length in the ATENA 2D environment [80].

5. Discussion of the results and validation of the GAM

This section aims to show and discuss the results obtained from the GAM and compare them with the numerical results. Based on those comparisons, the GAM is validated. To facilitate that, the present section is divided into four subsections where the results of the bonded joints with no anchorages, with anchorages with linear and nonlinear behaviours, and the combination of these, are presented.

5.1. Methodology followed for the validation of the GAM

The validation of the GAM is based on the load-slip curves obtained in each generated case previously identified in Table 1. Hence, the analytical load-slip curves are compared with their corresponding homologous numerical curve obtained from the Finite Element Method (FEM). The Integral Absolute Error (IAE) is calculated for each generated case. The IAE is known to be a sensitive parameter to the deviation of a theoretical result from experimental data, and it has been used for model assessment in other studies available in the literature, e.g. [62,82,83]. The IAE is calculated as follows:

$$IAE = \sum_{s=1}^{n} \frac{|d^{GAM} - d^{FEM}|}{\sum_{s=1}^{n} d^{FEM}} \tag{30}$$

where d^{GAM} and d^{FEM} correspond to the data obtained from the GAM and those calculated from the FEM, respectively; and n corresponds to the number of measurements carried out during the simulations of the debonding process.

It should be noted that the analytical simulations or the numerical simulations did not consider the rupture of the CFRP composite or the rupture of the springs, so the IAE values could be determined until 4 mm of slip at the loaded end of the CFRP-to-concrete joints. For this reason, no considerations about the failure mode of the generated bonded joints (e.g., complete debonding, rupture of the CFRP composite or rupture of the anchorages) are made.

Alternatively to the IAE, some results obtained from the GAM are also compared with those obtained from the numerical simulations. Beyond the calculated IAE values, the loads transmitted to the CFRP composite predicted by the GAM are compared with those numerically obtained, and the results were calculated according to:

$$Dev. = \frac{F_i^{GAM} - F_i^{FEM}}{F_i^{FEM}} \times 100\% \tag{31}$$

where F_i^{GAM} and F_i^{FEM} are the loads corresponding to the debonding of the joint and the maximum load reached in the GAM and the numerical simulation, respectively.

5.2. Assuming no springs

Fig. 7 shows the load-slip curves obtained from the generated cases with no springs, i.e., the reference cases. As expected, the load-slip curves follow the same trend known in the literature, e.g. [2,5–8,84]. Thus, when the bonded length is short, the loads transmitted to the CFRP

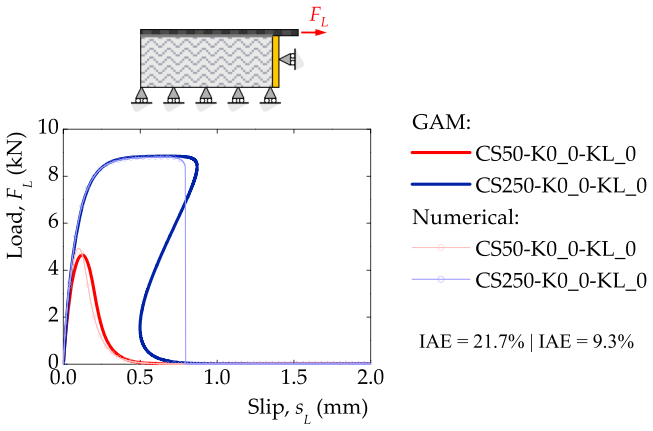

Fig. 7. Load-slip curves obtained in the reference cases (with no springs).

composite are smaller than in the case with the longest bonded length, in which the bonded length is longer than the effective bond length. In both generated cases, the initial ascending branches of the load-slip curves have a nonlinear trend and are quite similar. In the case of the generated case CS250-K0_0-KL_0, a plateau at maximum load can be seen in both models, i.e., GAM and numerical. However, only the GAM was able to predict the snap-back phenomenon. This is justified by the use of the Newton-Raphson method in the numerical simulation, which prevents the capture of the snap-back phenomenon in the generated case CS250-K0_0-KL_0.

The accuracy of the generated case CS50-K0_0-KL_0 is lower than that in the generated case CS50-K0_0-KL_0, where the calculated IAEs are 21.7 % and 9.3 %, respectively. These two reference cases had the highest IAE values of the generated cases under study due to the relatively low loads transmitted to the CFRP composite when compared with the other cases. Hence, the GAM predicted a maximum load in both cases of 4.64 kN and 8.85 kN in specimens CS50-K0_0-KL_0 and CS250-K0_0-KL_0, respectively, whereas the numerical simulation reached 4.92 kN and 8.85 kN, respectively. A deviation of − 5.7 % was determined for specimen CS50-K0_0-KL_0, while no deviation was determined at all for specimen CS250-K0_0-KL_0.

5.3. *Combining no springs with springs with linear and nonlinear behaviour*

In this subsection, the generated cases with an end and a loaded anchorage are reported. Fig. 8 shows all the studied cases with a bonded length of 50 mm under those circumstances where the following four different cases are considered: (a) using the U-wrap anchorage as an end anchorage (see Figs. 8a and 9a); (b) using the U-wrap anchorage as a loaded anchorage (see Figs. 8b and 9b); (c) using the transversely compressed mechanical anchorage as an end anchorage (see Figs. 8c and 9c); and (d) using the transversely compressed mechanical anchorage as a loaded anchorage (see Figs. 8d and 9d).

In the cases where the spring has linear behaviour (i.e. considering the U-wrap anchorage), a meaningful linear branch is seen (see Figs. 8a and 8b). This shows how relevant the anchorage is when the CFRP-to-concrete joint is short. However, it should be noted that the rupture of the CFRP composite can be achieved for a low slip magnitude. Moreover, if the stiffness of the anchorage is high, the rupture of the CFRP

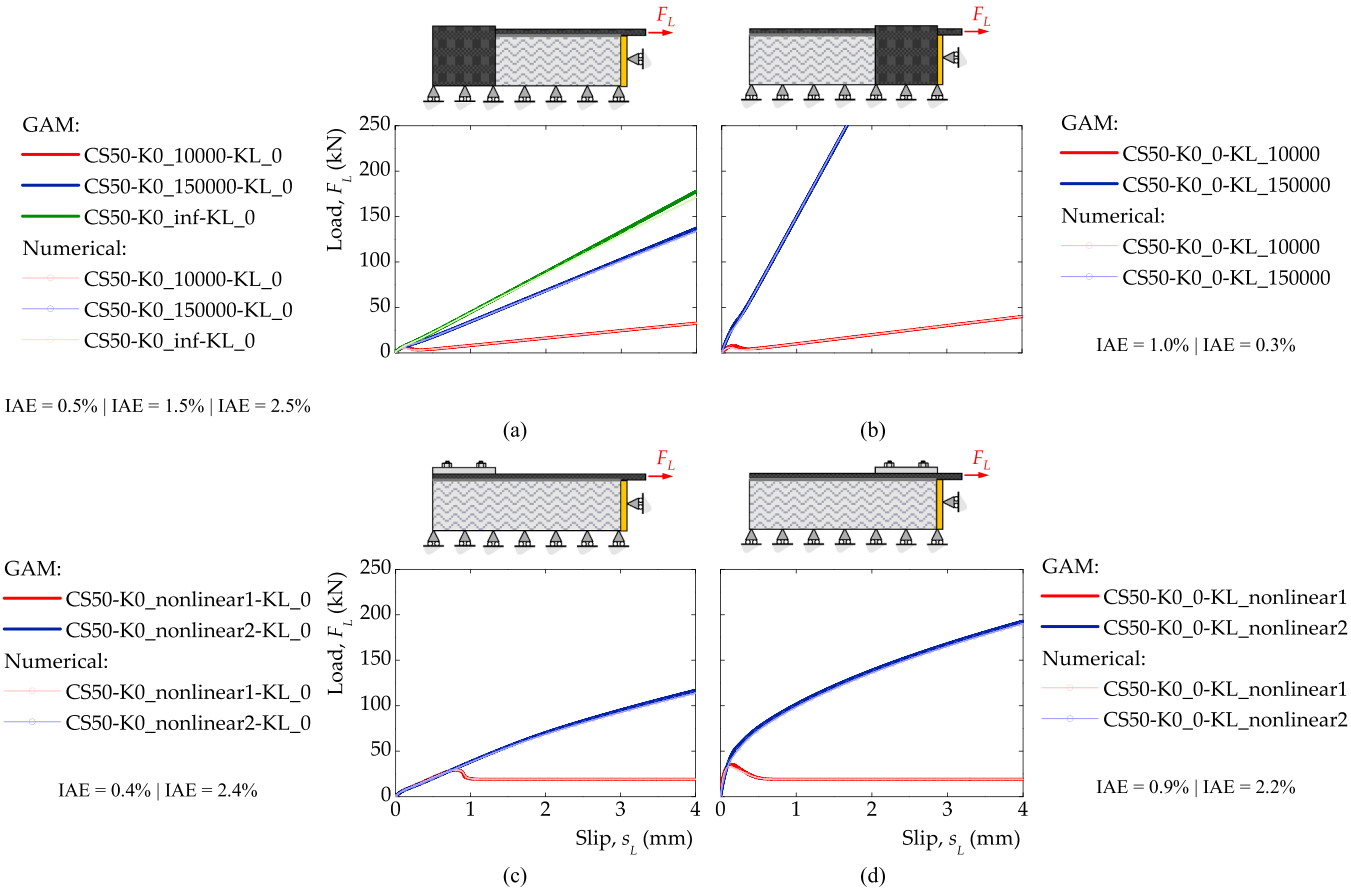

Fig. 8. Load-slip curves obtained in the cases with a short bonded length of 50 mm with: (a) a spring with a linear behaviour as an end anchorage; (b) a spring with a linear behaviour as a loaded anchorage; (c) a spring with a nonlinear behaviour as an end anchorage; and (d) a spring with a nonlinear behaviour as a loaded anchorage.

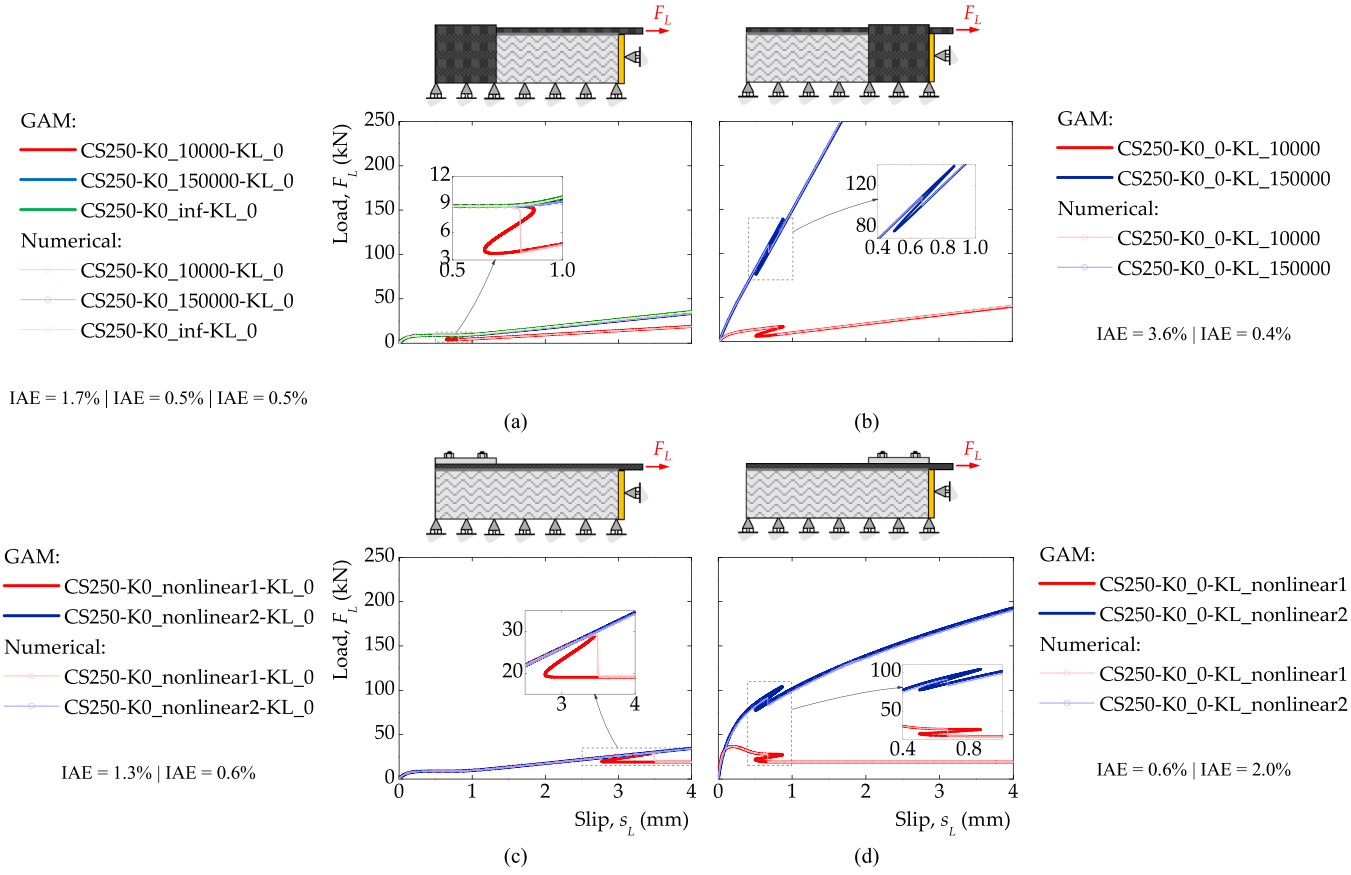

Fig. 9. Load-slip curves obtained in the cases with a short bonded length of 250 mm with: (a) a spring with linear behaviour as an end anchorage; (b) a spring with linear behaviour as a loaded anchorage; (c) a spring with nonlinear behaviour as an end anchorage; and (d) a spring with nonlinear behaviour as a loaded anchorage.

composite can be achieved sooner since the slope of the load-slip curve is higher than in those cases where the stiffness of the anchorage is lower. The same can be stated when the anchorage is installed at the loaded end, i.e. as a loaded anchorage. In this case, there is a more accentuated increase in the slope of the load-slip curve for higher stiffnesses of the loaded anchorage (see Fig. 8b).

Similar behaviour can be observed when the anchorage has nonlinear behaviour (i.e., considering the transversely compressed mechanical anchorage). Thus, when a long anchorage with a higher performance is used, the CFRP-to-concrete joints have a better bond performance, reaching higher maximum loads than the joints with a short anchorage and lower bond performance. Since the short anchorage shows a residual load (see Fig. 5) due to the friction between the CFRP and the concrete, after the full debonding of the CFRP composite from the substrate, a residual load is observed in these specimens (see Figs. 8c and 8d). On the other hand, using a long anchorage there is a continuous increase of the load with the slip, with a similar nonlinear trend of the long anchorage. Still, for a low slip magnitude, the differences of the load-slip curves observed between using a short or a long anchorage are marginal, which means that if the CFRP rupture is achieved within that slip magnitude, then the choice between a long or short anchorage is almost irrelevant.

In all the cases shown in Fig. 8, the IAE values stayed between 0.3 % in specimen CS50-K0_0-KL_150000 and 2.5 % in specimen CS50-K0_inf-KL_0, which shows the high level of accuracy of the GAM with the numerical results regardless of the anchorage type, i.e., with a linear or nonlinear behaviour, and the place where it is installed (at the unpulled or pulled CFRP end). It should also be noted that since the bonded length of the joints is short, no snap-back is observed in these cases, as shown in Fig. 8. Therefore, these results suggest that the anchorage type does not influence the appearance of the snap-back phenomenon.

Fig. 9 shows all the studied cases with a bonded length of 250 mm with an end and a loaded anchorage. Like the specimens with a short-bonded length, a major linear branch can be seen from the specimens where a spring with a linear behaviour is used, while a nonlinear branch is observed from the load-slip curve of the specimens with an anchorage with nonlinear behaviour. The main differences that can be observed are the presence of the snap-back phenomenon in all the curves and the initial branch where the CFRP debonding takes place on a larger bonded length. For instance, in the generated case CS250-K0_nonlinear1-KL_0 (see Fig. 9c), a first plateau at approximately 8.7 kN can be observed. Then, the load increases until the snap-back occurs when the load transmitted to the CFRP composite is approximately 29.3 kN. Due to the frictional stage of the short anchorage (see Fig. 5), the loads tend to the same residual load value of 19.0 kN. The main difference between the CS250-K0_0-KL-nonlinear1 and CS250-K0_0-KL-nonlinear2 (shown in Fig. 9d) is the higher debonding load reached in the latter case of approximately 36.5 kN, which is the same value analytically and numerically obtained. However, the snap-back occurs at a lighter load, i.e., at approximately 27.4 kN.

5.4. *Combining springs with linear and nonlinear behaviour*

The results obtained by combining the linear and nonlinear behaviours of the anchorages are reported below. The results were grouped into four different cases: (a) using the U-wrap anchorage as an end and loaded anchorage (see Figs. 9a and 10a); (b) using the U-wrap anchorage as an end anchorage and the transversely compressed mechanical anchorage as a loaded anchorage (see Figs. 9b and 10b); (c) using the transversely compressed mechanical anchorage as an end anchorage

and the U-wrap anchorage as a loaded anchorage (see Figs. 9c and 10c); and (d) using the transversely compressed mechanical anchorage as an end and loaded anchorage (see Figs. 9d and 10d).

As expected, the bond performance of these particular bonded joints is improved when compared with those discussed in the previous subsections due to the use of two anchorages rather than only one. Considering the results obtained from the cases with the shortest bonded lengths, it can be stated that using the CFRP U-wrap anchorage as an end anchorage (see Fig. 10b), its influence is more relevant when the short transversely compressed anchorage is used as a loaded anchorage, e.g. cases CS50-K0_10000-KL_nonlinear1 and CS50-K0_150000-KL_nonlinear1. Otherwise, the nonlinear behaviour of the transversely compressed anchorage overlaps the linear behaviour of the CFRP U-wrap anchorage (see cases CS50-K0_10000-KL_nonlinear2 and CS50-K0_150000-KL_nonlinear2). When this anchorage sequence is changed, i.e. using the transversely compressed anchorage and the CFRP U-wrap anchorages as an end and loaded anchorages, respectively, the load-slip curves of the corresponding bonded joints change. Under these circumstances, the debonding loads tend to increase, namely in the cases where the stiffer CFRP U-wraps are used as a loaded anchorage, i.e. in CS50-K0_nonlinear1-KL_150000 and CS50-K0_nonlinear2_KL_150000 (see Fig. 10d), but after that debonding load point, their corresponding load-slip curves are quite similar to those shown in Fig. 10a.

Using two long transversely compressed anchorages as an end and loaded anchorage (see Fig. 10d) led, as expected, to the highest bond performance of the CFRP-to-concrete joints. For a lower load magnitude, the four load-slip curves are similar, but the debonding initiation occurs first in the cases where the short transversely compressed anchorage is used as a loaded anchorage, i.e. in case CS50-K0_nonlinear1-KL_nonlinear1 and CS50-K0_nonlinear2-KL_nonlinear1. Only in CS50-K0_nonlinear1-KL_nonlinear1 is a plateau with a residual load of 38.0 kN seen. This value is twice the value of the plateau of the load-displacement curve of the short transversely mechanical anchorage shown in Fig. 5. Therefore, when the end and load anchorages are used, after the CFRP debonding, the anchorage is within a parallel configuration. This can be explained by considering that after the CFRP debonding, the interfacial slips along the CFRP-to-concrete interface tend to the same value [2,5–8], and so, the slips at the end and loaded anchorages are the same, but the loads may be different. For instance, the slopes of the load-slip curves of the cases with a CFRP-wrap anchorage shown in Figs. 10a or 10b can be determined by the sum of the stiffnesses of each case with only one anchorage, i.e., with only an end or loaded anchorage as shown in Fig. 8.

When compared with the corresponding load-slip curves, the accuracy of the GAM is quite good. The calculated IAE values varied from only 0.1 % (in the generated case CS50-K0_150000-KL_150000) to 2.2 % (in the generated case CS50-K0_nonlinear2-KL_nonlinear2). Once again, since the bonded length of the joints is short, no snap-back phenomenon is observed in any of the load-slip curves shown in Fig. 10, regardless of the anchorage type or combination type.

Fig. 11 shows the load-slip curves of the cases with a bonded length of 250 mm. Like the cases shown in Fig. 10, the best bond performance can be observed in the cases where a loaded anchorage with the highest stiffness is used. The snap-back phenomenon can now be observed in the

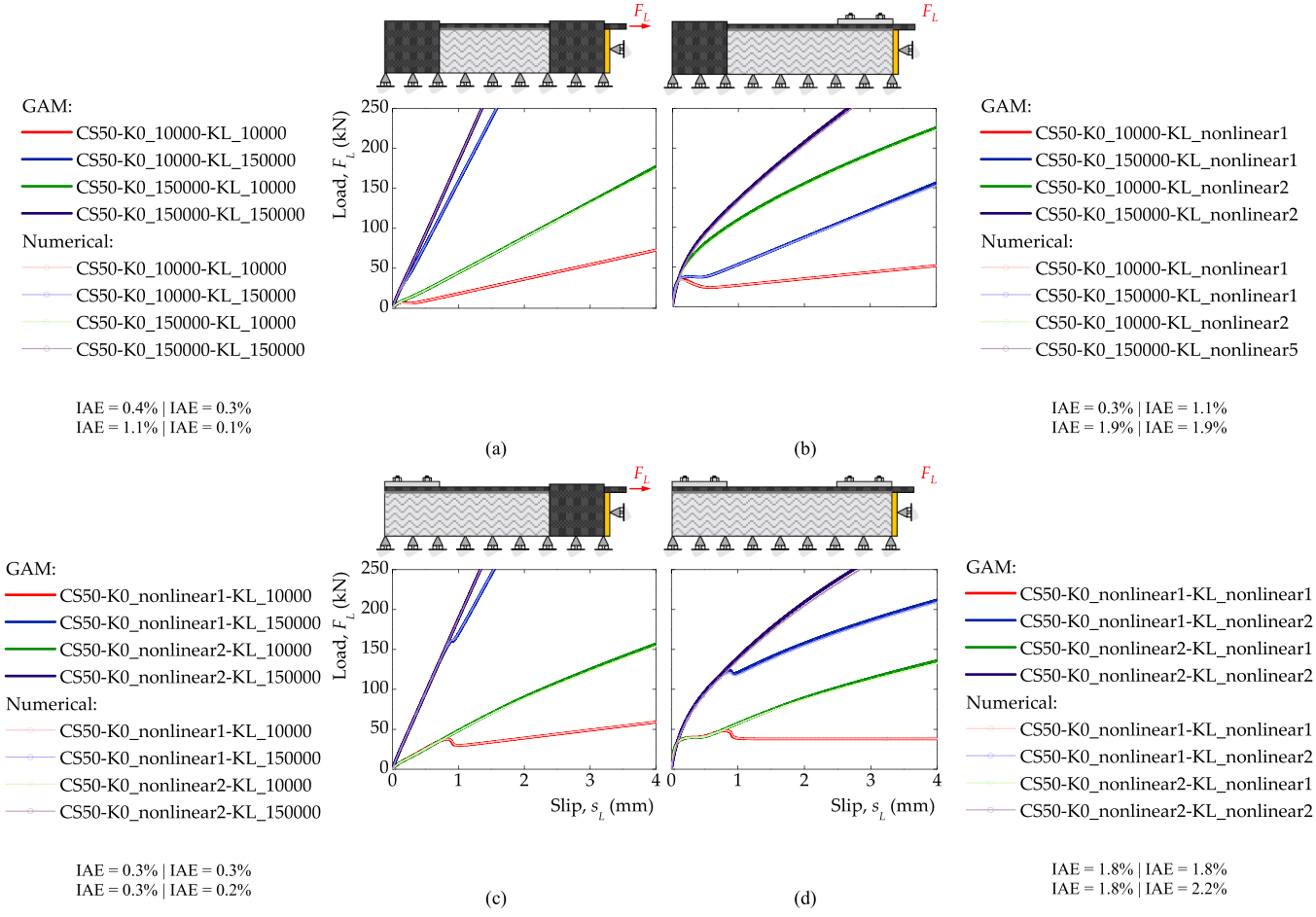

Fig. 10. Load-slip curves obtained in the cases with a long bonded length of 50 mm with: (a) springs with linear behaviour as an end and loaded anchorage; (b) a spring with linear and nonlinear behaviour as an end and loaded anchorage, respectively; (c) a spring with nonlinear and linear behaviour as an end and loaded anchorage, respectively; and (d) springs with nonlinear behaviour as an end and loaded anchorage.

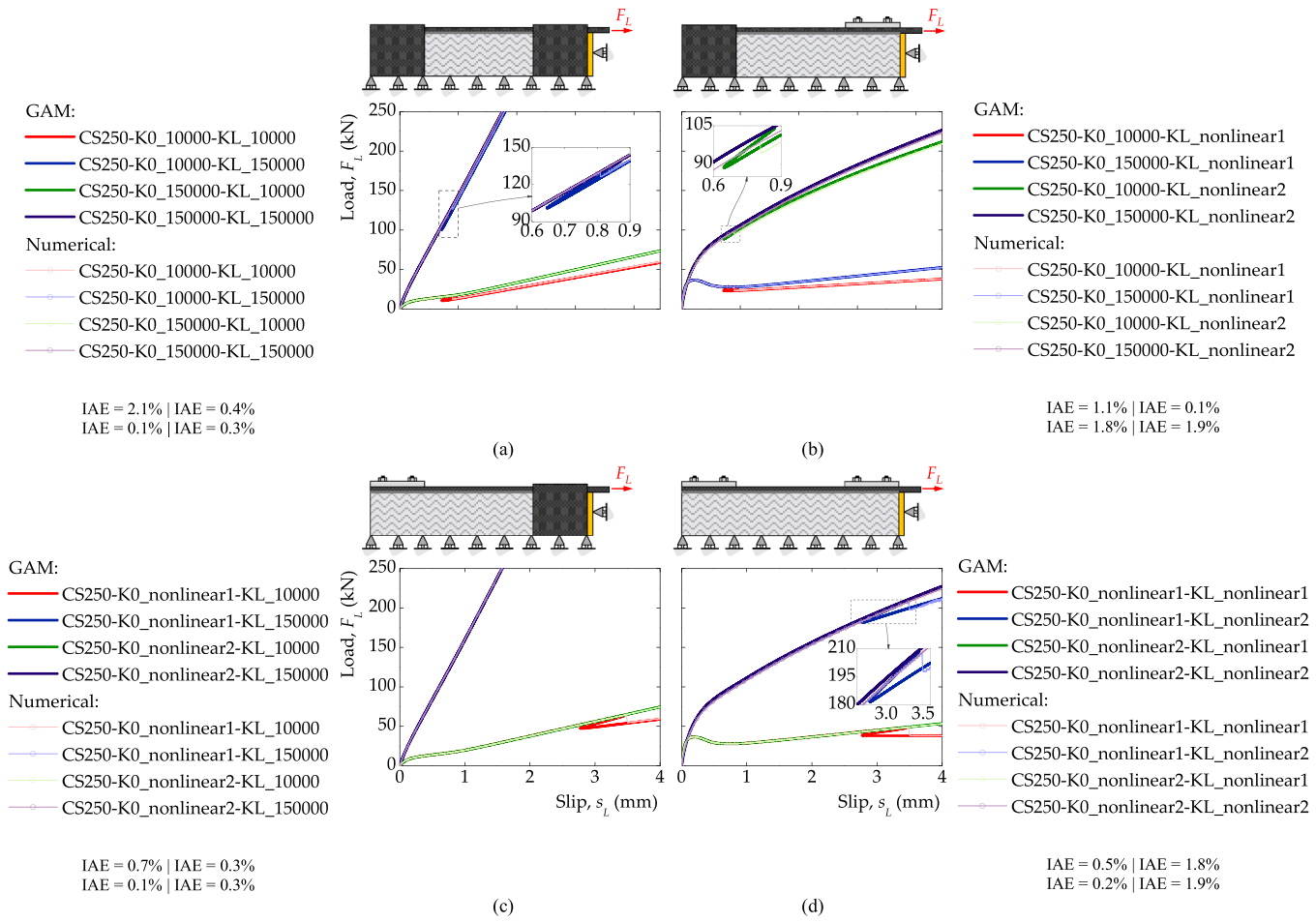

Fig. 11. Load-slip curves obtained in the cases with a long bonded length of 250 mm with: (a) springs with linear behaviour as an end and loaded anchorage; (b) a spring with linear and nonlinear behaviour as an end and loaded anchorage, respectively; (c) a spring with nonlinear and linear behaviour as an end and loaded anchorage, respectively; and (d) springs with nonlinear behaviour as an end and loaded anchorage.

slip range shown in Fig. 11. As already mentioned in the previous subsection, this snap-back phenomenon only occurs, once again, in these cases where the bonded length is longer than the effective bond length, regardless of the anchorage type used and the place of installation on the bonded length. In the cases CS250-K0_nonlinear1_KL_10000 and CS250-K0_nonlinear1_KL_nonlinear1, the maximum loads developed before the snap-back are approximately 62.4 kN and 48.3 kN, respectively. Since the stiffnesses of the anchorages are higher than those in the previously mentioned two cases, the peak loads before the snap-back in cases CS250-K0_10000-KL_nonlinear2 and CS250-K0_nonlinear1-KL_nonlinear2 are 104.2 kN and 208.8 kN, respectively. After that, the loads transmitted to the CFRP composite continue to increase with the slips.

Once more, the calculated IAE values in these cases are quite low, varying between 0.1 % in case CS250-K0_150000-KL_10000 and 2.1 % in case CS250-K0_10000-KL_10000, which shows the high level of accuracy of the GAM compared to the numerical simulations. It should only be noted that the highest differences between the analytical and numerical load-slip curves are observed at the snap-back region, where the numerical simulations cannot capture this phenomenon due to the use of the Newton-Raphson method in solving the nonlinear equations of the numerical problem. Nevertheless, this did not contribute to a significant increase in the IAE values of all these generated cases.

6. Comparisons with other studies

In this section, the GAM is compared with some results found in the literature. The work carried out by Zhang and Smith [31], Codina et al. [32] and the results obtained from the generated data assumed by Huang et al. [33] were considered. In the first study, the authors [31] used CFRP spike anchors to improve the bond performance of CFRP-to-concrete bonded joints, whilst the second study used a transversely compressed mechanical anchorage as an end anchorage. In the third study, the authors [33] considered three different cases and generated data to analytically predict the bond performance of CFRP-to-concrete bonded joints of a: (i) CFRP U-wrap anchorage; (ii) CFRP spike anchorage; and (iii) transversely compressed mechanical anchorage. In this third study, all three cases considered the bond behaviour of the CFRP-to-concrete joints with an end or loaded anchorage. In the following subsections, more details are reported, but to obtain more details and insights into these works, the reader is advised to refer to the original studies.

6.1. Tests carried out by Zhang and Smith [31]

Zhang and Smith [31] carried out an experimental study on the bond behaviour of the mechanically anchored CFRP-to-concrete joints with CFRP spike anchors. The authors [31] tested three different series of mechanically anchored CFRP-to-concrete joints and one more with no anchorages, where the results were used for reference purposes. They also considered the influence of the CFRP spike anchor position on the CFRP-to-concrete joint and defined its load-displacement response according to the elastic-plastic behaviour shown in Fig. 12.

Zhang and Smith [31] used a CFRP sheet with a nominal thickness of

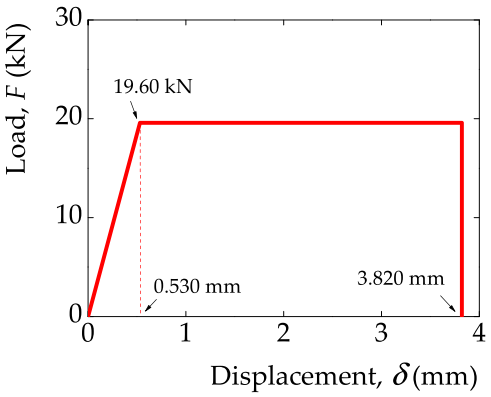

Fig. 12. Load-displacement curves associated with the CFRP-to-concrete bonded joints with a CFRP spike anchor as defined by Zhang and Smith [31].

0.131 mm and 50 mm wide. Two CFRP rolls were used, and from the test of five flat coupons, the second CFRP roll led to the following average mechanical properties: tensile strength of 2978 MPa, rupture strain of 1.34 % and elastic modulus of 227 GPa. The CFRP sheets were externally bonded onto a concrete block measuring 200 mm × 200 mm × 400 mm (thickness × width × length). The concrete strength was reported as being equal to 55 MPa, and it was determined from the tests of concrete cubes. Although the elastic modulus was not reported, the elastic modulus was estimated through the Eurocode 2 [66] formulae, leading to approximately 35.0 GPa.

Based on the work carried out by Zhang and Smith [31], Dong et al. [85] have also simulated the bond behaviour of specimen B7–2, i.e. from series B [31]. For this reason, this particular specimen was analysed. This specimen is300 mm long, and the CFRP spike anchor was installed 125 mm from the CFRP unloaded end (or 175 mm from the CFRP pulled end). Thus, two approaches were considered. The first one considered a bonded length of 175 mm with an end anchorage simulated by a linear spring whose definition was calibrated by the GAM. The second one considered the load-displacement response of the CFRP spike anchor shown in Fig. 12, which was reported by Zhang and Smith [31] and the proposed methodology shown in Fig. 4 was followed. Thus, Fig. 13a shows the first case where the spring with linear behaviour considered the 125 mm of the CFRP-to-concrete joint and the CFRP spike anchor as a loaded anchorage, and then, the CFRP-to-concrete joint with this end anchorage was solved, resulting in an equivalent configuration where the spring has a stiffness of 90000 N/mm with a rupture displacement of 0.365 mm. Fig. 13b shows the second case, i.e., considering all the steps shown in Fig. 4 and the CFRP spike anchor placed at 125 mm from the CFRP unpulled end.

In both cases, the results are fairly consistent with the experiments and with the predictions made by Dong et al. [85]. However, Dong et al. [85] predicted a lower maximum load transmitted to the CFRP sheet than the experiment. The GAM, assuming a spring with linear behaviour, showed a small decrease in the load after the debonding of the CFRP from the concrete, and then the load increased linearly once again until the complete failure of the CFRP-to-concrete joint. In this case, the predicted maximum load is 32.94 kN, which is 12.7 % higher than the maximum load obtained by Zhang and Smith [31] (29.24 kN). On the other hand, when the load-displacement of a single CFRP anchor is considered, the load-slip curve predicted by the GAM follows the curve obtained by Dong et al. [85] quite closely. However, the GAM shows a maximum load of 5.7 % lower than that experimentally obtained by Zhang and Smith [31], i.e. 27.57 kN. After that, the snap-back phenomenon is observed, and the complete failure of the specimen is not reached because of the plastic behaviour of the CFRP spike anchor (see Fig. 12).

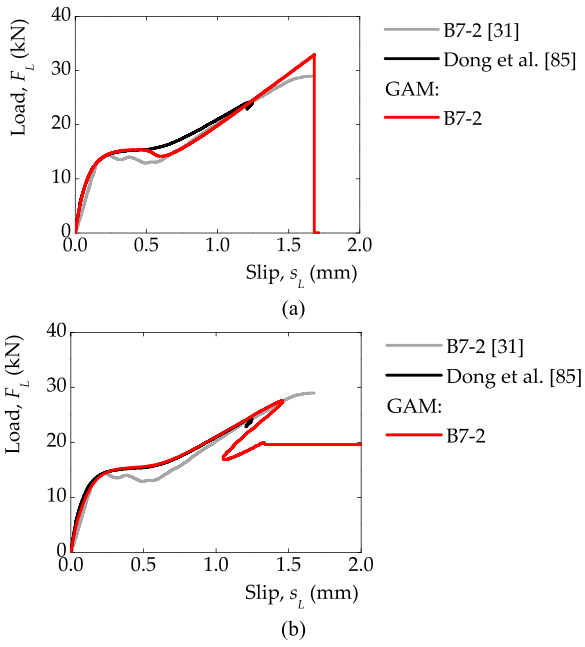

Fig. 13. Comparison between the load-slip curves of the CFRP-to-concrete joints obtained by the GAM with those obtained by Dong et al. [85] and Zhang and Smith [31]: (a) assuming an end anchorage with linear behaviour; and (b) assuming that the CFRP spike anchor has linear behaviour with a stiffness of 36980 N/mm and a rupture displacement of 0.685 mm.

6.2. *Tests carried out by Codina et al. [32]*

Among a series of flexural tests on reinforced concrete (RC) beams externally bonded with CFRP composites, Codina et al. [32] carried out six single lap-shear tests with CFRP composites externally bonded to concrete. In these latter tests, the authors [32] considered three different cases: (i) with no anchorages and a bonded length of 250 mm (originally denoted as EB_250); (ii) with a π-shape transversally compressed mechanical anchorage and an anchorage length of 50 mm installed at the centre of the bonded length of the CFRP-to-concrete joint with a total length of 250 mm (denoted as HB_250); and (iii) only the transversely compressed mechanical anchorage bonded with an anchorage length of 50 mm (denoted as HB_50). Six CFRP strips 50 mm wide and 1.4 mm thick, were externally bonded to six concrete blocks measuring 200 mm × 200 mm × 370 mm (thickness × width × length), i.e., each case was repeated once. However, in the case of the HB_50 specimens, the load-slip curve obtained in the first test was reported by Codina et al. [32].

The mechanical properties of CFRP composite were not determined by the authors [32], and the following mechanical properties given by the manufacturer were considered: tensile strength of 2800 MPa, elastic modulus of 170 GPa, and a rupture strain of 1.6 %. The mechanical properties of the concrete were determined from the uniaxial test of three concrete cylinders with a diameter of 150 mm and 300 mm high, leading to a mean concrete strength of 45.98 MPa, which corresponds to a mean tensile strength of 3.94 MPa and an elastic modulus of 36.21 MPa. The thixotropic S&P resin 220 HP was used to bond the CFRP strips onto the concrete. Like the CFRP strips, the resin was not tested, and the mechanical properties given by the manufacturer were considered, i.e., a tensile strength of 15 MPa and an elastic modulus of 7.10 GPa after a curing time of seven days.

From the tests of the EB_250 specimens, the bond-slip relationship of the CFRP-to-concrete joints was approximated to a bilinear shape with a maximum shear stress of 12.70 MPa with a corresponding slip of 0.030 mm and a final slip, i.e. beyond which no further shear bond stress is transferred within the CFRP-to-concrete interface, of 0.180 mm. This

triangular bond-slip relationship was approximated to the exponential bond-slip relationship defined in Eq. (1) through a minimisation process where mode II fracture energy was used as a constraint, leading to $B = 21.796\ \text{mm}^{-1}$.

Fig. 14 compares the load-slip curves obtained by the GAM of the EB_250 and HB_250 specimens with those experimentally obtained by Codina et al. [32]. The load-slip curve of specimen HB_50 was used to simulate the loaded anchorage as explained in Subsection 2.2 (see Fig. 4b.i). In addition, the numerical load-slip curve of the HB_250n specimen obtained by Codina et al. [32] is also shown in Fig. 14. As can be seen, the results obtained by the GAM are fairly consistent with those obtained by Codina et al. [32]. In the case of the EB_250 specimen, the maximum load transmitted to the CFRP composite was approximately 40.1 kN, whereas the GAM predicted a maximum load of 37.1 kN, which represents a deviation of approximately − 7.5 %. However, a higher deviation was analytically predicted for specimen HB_250, i.e., the experimental maximum load transmitted to the CFRP composite was 55.0 kN, whereas the GAM predicted 65.5 kN (a deviation of 19.1 %). This higher deviation is consistent with the numerical result obtained by Codina et al. [32], who predicted a maximum load of approximately 60.8 kN, corresponding to a deviation of approximately 10.6 %. In the GAM and numerical models, both post-peak behaviours are consistent since the loads have the same residual value, i.e., the same as the test of the HB_50 specimen of 19.0 kN. Unlike the numerical simulation of Codina [32], the GAM captured the snap-back phenomenon, allowing the understanding of the full debonding process of the mechanically anchored joint HB_250.

6.3. Generated data by Huang et al. [33]

Unlike the previous studies, the use of a loaded anchorage is quite uncommon. Nevertheless, Huang et al. [33] studied the bond performance of CFRP-to-concrete joints with a loaded anchorage and developed an analytical model based on a triangular bond-slip relationship. The analytical model is quite complicated since it requires the use of a different equation to define all the states that the bonded joint undergoes until its complete debonding or rupture. To validate the analytical model, the authors [33] compared their results with those obtained from the FEM. Huang et al. [33] considered three different loaded anchorages: CFRP U-jacketing, CFRP spike anchors and mechanical fasteners with a lower and higher torque level. Huang et al. [33] assumed a spring with linear behaviour to simulate the CFRP-to-concrete joints with the U-jacketing. In the case of the CFRP spike anchors, the elastic-plastic behaviour was considered, which was justified by the numerical data reported by Yang et al. [86]. Two different models were considered for the mechanical fasteners with a lower and a higher torque. Like the CFRP spike anchors, a spring with elastic-plastic behaviour could model the mechanical fasteners with a lower torque, whereas a spring with linear behaviour with fragile rupture could model the mechanical fasteners with a higher torque. Fig. 15 shows these three models considered in the work developed by

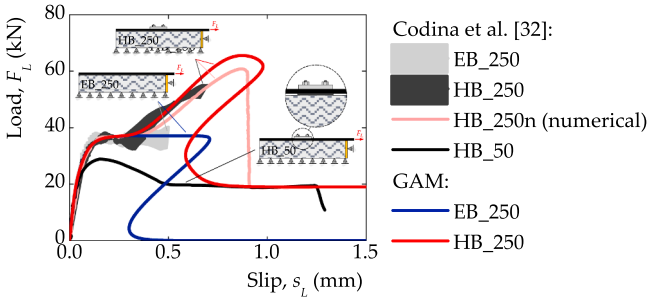

Fig. 14. Comparison between the load-slip curves of the CFRP-to-concrete joints obtained by the GAM with those tested by Codina et al. [32].

Huang et al. [33].

The CFRP-to-concrete joints with the U-jacketing as a loaded anchorage had a unidirectional CFRP composite which was 1.2 mm thick and 50 mm wide, and it was externally bonded to a concrete block with a cross-sectional area of 300 × 220 mm (thickness × width). Since Huang et al.'s [33] analytical model cannot deal with short bonded lengths, a bonded length of 400 mm was assumed, which is longer than the effective bond length of 176 mm, as reported by Huang et al. [33]. The elastic modulus of the CFRP composite is 205 GPa, whilst the elastic modulus of the concrete is 33 GPa. The triangular bond-slip relationship was defined as follows: $\tau_{b,\max} = 5.59$ MPa with a corresponding slip of 0.073 mm, ultimate slip of 0.280 mm and a mode II fracture energy of 0.783 N/mm. This triangular bond-slip relationship was adjusted to the exponential bond-slip relationship defined in Eq. (1) through a minimisation process where the fracture energy was used as a constraint. As a result, the stiffness index of the CFRP-to-concrete bonded joint is $B = 12.739\ \text{mm}^{-1}$.

Figs. 16–18 compare the results obtained from the GAM with those obtained by Huang et al. [33]. From an overall overview, it can be said that the GAM agrees well with the generated data of Huang et al. [33]. In the cases of the CFRP U-jacket anchorage and CFRP spike anchorages shown, respectively, in Figs. 16 and 17, the load-slip curves obtained by the GAM agree perfectly with the debonding load as well as the rupture load reached in the CFRP-to-concrete joints with an end or loaded anchorage (see Fig. 16). The load increase observed during the debonding process of the CFRP composite from the concrete in the U-jacket loaded anchorage has the same slope of the post-peak behaviour (see Fig. 16). This can be explained by considering the equilibrium of the CFRP composite. The total load transmitted to the CFRP composite corresponds to the sum of the shear bond stresses developed throughout the bonded length plus the load in the loaded anchorage. Since with no anchorages a plateau at maximum load can be seen, the influence of the loaded anchorage in this part of the debonding process is reflected in the bonded joint with a load increase rather than a plateau due to the sum of the loads in the loaded anchorage. With or without a loaded anchorage, the corresponding slope is the same as that observed in the post-peak curve. So, in the case of no anchorage, the post-peak behaviour of the bonded joint corresponds to a nil slope with no loads transmitted to the CFRP composite, whilst the joint with the loaded anchorage has a slope corresponding to the loaded anchorage stiffness. In the case shown in Fig. 16, the failure occurs when the maximum displacement of the loaded anchorage of 4.300 mm (see Fig. 15) is reached. Although using the U-jacket as a loaded anchorage increases the debonding load, the failure of the mechanically anchored CFRP-to-concrete joints occurs at the same load of approximately 52.3 kN. However, the ductility of the CFRP-to-concrete joint with the end anchorage is reduced since the failure of the CFRP-to-concrete joint with the end anchorage occurs when the slip is 6.000 mm.

Like the CFRP-to-concrete bonded joints with a CFRP U-jacket or CFRP spike anchor, the CFRP-to-concrete joints with a transversely compressed end anchorage agreed well with the generated data provided by Huang et al. [33] (see Fig. 18). However, relevant differences can be found when the CFRP-to-concrete bonded joints with a transversely compressed loaded anchorage are considered. The results reported by Huang et al. [33] seem not to respect the maximum displacement of the anchorage, as shown in Fig. 15c. For instance, in the case of the SA7 specimen with a loaded anchorage, when the slip reaches the maximum elastic displacement of the anchorage of 0.378 mm, Huang et al.'s [33] model seems to ignore that. The loads transmitted to the CFRP composite continue increasing, whereas the GAM shows a plateau at 16.25 kN until the rupture of the CFRP spike anchorage at 0.588 mm (see Fig. 18a). Despite being the same maximum displacement reached in Huang et al.'s [33] model, higher slips can be found in the load-slip curve, e.g., at maximum load, the slip is approximately 0.842 mm, which is higher than the limit of the transversely compressed anchorage (see Fig. 15c). Similarly, for the SA10 specimen with a loaded

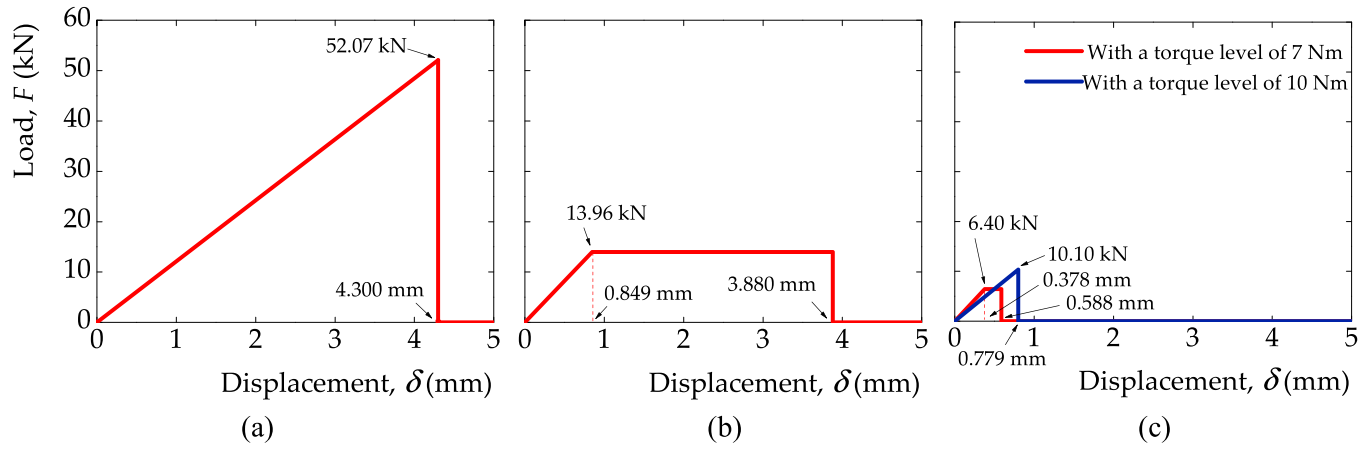

Fig. 15. Load-displacement curves associated with the CFRP-to-concrete bonded joints with a: (a) CFRP U-jacketing; (b) CFRP spike anchor; and (c) mechanical fastener (based on Huang et al.'s descriptions [33]).

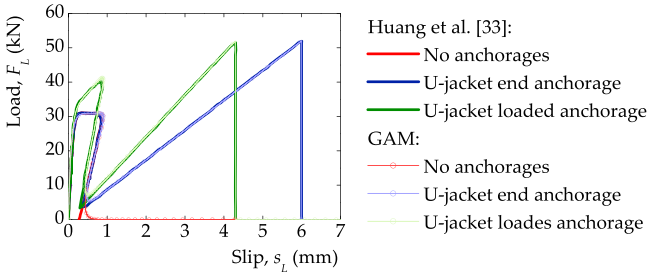

Fig. 16. Load-displacement curves associated with the CFRP-to-concrete bonded joints with a CFRP U-jacketing.

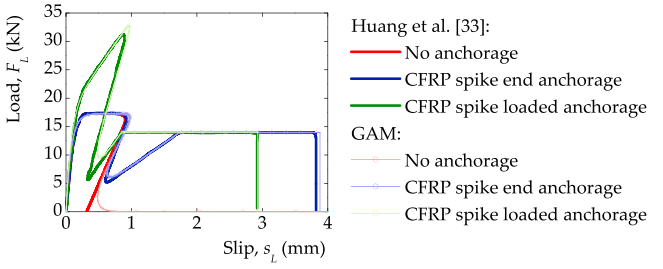

Fig. 17. Load-displacement curves associated with the CFRP-to-concrete bonded joints with a CFRP spike anchor.

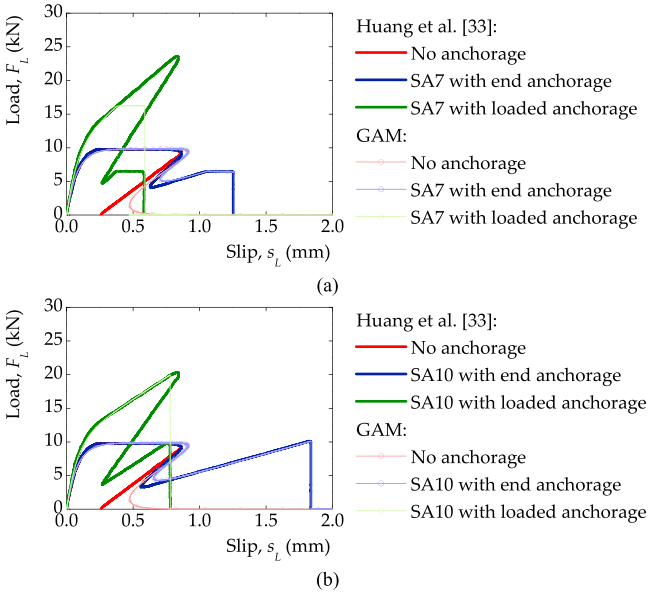

Fig. 18. Load-displacement curves associated with the CFRP-to-concrete bonded joints with a mechanical fastener with a torque of: (a) 7.0 Nm; and (b) 10.0 Nm.

anchorage (see Fig. 18b), Huang et al.'s [33] model seems to ignore, once again, the maximum displacement of the anchorage of 0.779 mm as shown in Fig. 15c. In this case, at the maximum load transmitted to the CFRP composite, a slip of approximately 0.866 mm is reached, which, again, is higher than the displacement limit of the transversely compressed anchorage of 0.779 mm (see Fig. 15c). Still, the GAM closely follows Huang et al.'s [33] model until 0.779 mm when the analytical simulation of the SA10 specimen predicts its collapse.

7. Conclusions

The current study proposes a generalised analytical model (GAM) able to predict the bond performance of innumerable FRP-to-substrate joints with or without an anchorage installed somewhere on their bonded length. Its simplicity and good accuracy with the FEM allow us to reach the following main conclusions:

- The use of a loaded anchorage rather than an end anchorage increases the load capacity of the FRP-to-substrate joints. However, their ductility is reduced. An intermediate situation can be achieved by installing the anchorage somewhere along the bonded length of the bonded joint, which is also a case covered by the GAM;
- Using a loaded anchorage with high stiffness allows an increase in the maximum loads transmitted to the bonded joints. However, using two anchorages at the CFRP unpulled and pulled ends maximises the load capacity of the bonded joint. It should be noted, however, that the rupture of the CFRP composite may influence the decision to use one or two (or more) anchorages, and the GAM may facilitate that choice, avoiding additional costs and unnecessary work;
- The snap-back phenomenon is only captured in those cases where the bonded length is longer than the effective bond length of the joint, regardless of the anchorage type. Thus, the use of an additional anchorage has no influence on this phenomenon, which can be captured by the GAM;
- When compared with other experimental studies, the GAM was able to reproduce the experiments as well as the numerical or analytical

results with good accuracy. It can also be concluded that the failure of the bonded joints can be well predicted by the GAM, i.e., predicting the CFRP rupture, the complete debonding or the anchorage (spring) failure;

- The use of a π-shape anchorage installed somewhere along the bonded length of the FRP-to-substrate joint can also be analytically predicted by the GAM. The proposed methodology fairly predicted the experiment carried out by Codina et al. [32]. However, to that end, the knowledge of the load-slip curve of the π-shape anchorage is critical. Alternatively, the load-slip response of the region near the unpulled CFRP end can be approximated by a linear load-displacement relationship until failure. Therefore, the problem becomes easier to solve as an FRP-to-substrate joint with an end anchorage with linear behaviour.

CRediT authorship contribution statement

Hugo C Biscaia: Writing – original draft, Validation, Software, Project administration, Methodology, Investigation, Funding acquisition, Formal analysis, Data curation, Conceptualization.

Declaration of Competing Interest

The author declares the following financial interests/personal relationships that may be considered as potential competing interests: Hugo C. Biscaia reports that financial support was provided by the Foundation for Science and Technology.

Acknowledgments

The author is thankful to Fundação para a Ciência e Tecnologia (FCT-MCTES) for the partial funding of this work under the strategic projects UID/00667: Unidade de Investigação e Desenvolvimento em Engenharia Mecânica e Industrial (UNIDEMI).

Declaration of competing interest

The author declares that he has no known competing financial interests or personal relationships that could have influenced the work reported in this paper.

Data availability

Data will be made available on request.

References

[1] B. Zhang, H. Zhu, Z. Yang, Y.R. Dong, BFRP bars reinforced geopolymer-based coral aggregate concrete beams with sustainable and high seawater erosion resistance: flexural durability, economic, and ecological analysis, Eng. Struct. 330 (2025) 119910.
[2] H. Yuan, J.G. Teng, R. Seracino, Z.S. Wu, J. Yao, Full-range behavior of FRP-to-concrete bonded joints, Eng. Struct. 26 (5) (2004) 553–565.
[3] J.G. Dai, T. Ueda, Y. Sato, Development of the nonlinear bond stress-slip model of fiber reinforced plastics sheet-concrete interfaces with a simple method, J. Compos. Constr. 9 (1) (2005) 52–62.
[4] C. Mazzotti, M. Savoia, B. Ferracuti, An experimental study on delamination of FRP plates bonded to concrete, Constr. Build. Mater. 22 (7) (2008) 1409–1421.
[5] D. Fernando, T. Yu, J.G. Teng, Behavior of CFRP laminates bonded to a steel substrate using a ductile adhesive, J. Compos. Constr. 18 (2) (2013) 04013040.
[6] H.C. Biscaia, C. Chastre, A. Viegas, A new discrete method to model FRP–to-parent material bonded joints, Compos. Struct. 121 (2015) 280–295.
[7] H.C. Biscaia, I.S. Borba, C. Silva, C. Chastre, A nonlinear analytical model to predict the full-range debonding process of FRP-to-parent material interfaces free of any mechanical anchorage devices, Compos. Struct. 138 (2016) 52–63.
[8] C. Mazzotti, M. Savoia, B. Ferracuti, An experimental study on delamination of FRP plates bonded to concrete, Constr. Build. Mater. 22 (7) (2008) 1409–1421.
[9] H. Biscaia, C. Chastre, D. Cruz, N. Franco, Flexural strengthening of old timber floors with laminated carbon fiber reinforced polymers, J. Compos. Constr. 20 (1) (2017) 04016073.
[10] N. Franco, C. Chastre, H. Biscaia, Strengthening RC beams using stainless-steel continuous reinforcement embedded at ends, J. Struct. Eng. 146 (5) (2020) 04020065.
[11] A. Azevedo, J. Firmo, J. Correia, C. Chastre, H. Biscaia, N. Franco, Fire behaviour of CFRP-strengthened RC slabs using different techniques - EBR, NSM and CREatE, Compos. Part B Eng. 230 (2022) 109471.
[12] K. Narmashiri, M.Z. Jumaat, N.H.R. Sulong, Investigation on end anchoring of CFRP strengthened steel I-beams, Int. J. Phys. Sci. 5 (9) (2010) 1360–1371.
[13] C. Barris, L. Correia, J. Sena-Cruz, Experimental study on the bond behaviour of a transversely compressed mechanical anchorage system for externally bonded reinforcement, Compos. Struct. 200 (2018) 217–228.
[14] L. Correia, C. Barris, P. França, J. Sena-Cruz, Effect of temperature on bond behavior of externally bonded FRP laminates with mechanical end anchorage, J. Compos. Constr. 23 (5) (2019) 04019036.
[15] C. Mazzotti, M. Savoia, B. Ferracuti, A new single-shear set-up for stable debonding of FRP-concrete joints, Constr. Build. Mater. 23 (4) (2009) 1529–1537.
[16] H.C. Biscaia, C. Chastre, C. Silva, N. Franco, Mechanical response of anchored FRP bonded joints: a nonlinear analytical approach, Mech. Adv. Mater. Struct. 25 (3) (2018) 238–252.
[17] S. Zhao, J. Han, R. Guo, X. Feng, Digital-image based performance analysis of CFRP–concrete interface bond under anchorage, Structures 58 (2023) 105345.
[18] H.C. Biscaia, C. Chastre, M.A.G. Silva, Bond-slip model for FRP-to-concrete bonded joints under external compression, Compos. Part B Eng. 80 (2015) 246–259.
[19] H. Biscaia, C. Chastre, Design method and verification of steel plate anchorages for FRP-to-concrete bonded interfaces, Compos. Struct. 192 (2018) 52–66.
[20] H. Biscaia, P. Diogo, Experimental analysis of different anchorage solutions for laminated carbon fiber-reinforced polymers adhesively bonded to timber, Compos. Struct. 243 (2020) 112228.
[21] A. Mostafa, A.G. Razaqpur, CFRP anchor for preventing premature debonding of externally bonded FRP laminates from concrete, J. Compos. Constr. 17 (2013) 641–650.
[22] Y.F. Wu, K. Liu, Characterization of mechanically enhanced FRP bonding system, J. Compos. Constr. 17 (2013) 34–49.
[23] L. Gao, Q. Wei, Y. Huang, F. Zhang, Influence of anchor design parameters on flexural performance of hybrid bonded-fiber reinforced polymer strengthened reinforced, Structures 48 (2023) 1029–1045.
[24] E. Martinelli, A. Napoli, B. Nunziata, R. Realfonzo, Inverse identification of a bearing-stress-interface-slip relationship in mechanically fastened FRP laminates, Compos. Struct. 94 (8) (2012) 2548–2560.
[25] R. Realfonzo, E. Martinelli, A. Napoli, B. Nunziata, Experimental investigation of the mechanical connection between FRP laminates and concrete, Compos. Part B Eng. 45 (1) (2013) 341–355.
[26] C. Jiang, Q.Q. Yu, X.L. Gu, A unified bond-slip model for the interface between FRP and steel, Compos. Part B Eng. 227 (2021) 109380.
[27] H. Biscaia, D. Fernando, J.G. Dai, Prediction of the full debonding process of mixed-adhesive FRP-to-substrate joints through a new analytical method, Eng. Fract. Mech. 318 (2025) 110963.
[28] H.T. Wang, G. Wu, Bond-slip models for CFRP plates externally bonded to steel substrates, Compos. Struct. 184 (2018) 1204–1214.
[29] J. He, G. Xian, Y.X. Zhang, Numerical modelling of bond behaviour between steel and CFRP laminates with a ductile adhesive, Int. J. Adhes. Adhes. 104 (2021) 102753.
[30] A.S. Calabrese, T. D'Antino, P. Colombi, Effect of adhesive ductility on the bond behavior of CFRP-steel cohesive interfaces made with toughened epoxy resin, Compos. Sci. Technol. 257 (2024) 110824.
[31] H. Zhang, S.T. Smith, Influence of plate length and anchor position on FRP-to-concrete joints anchored with FRP anchors, Compos. Struct. 159 (2017) 615–624.
[32] A. Codina, L. Torres, T. D'Antino, M. Baena, C. Barris, Flexural performance of RC beams strengthened with HB CFRP plates: experimental study and theoretical model based on the intermediate crack debonding, Constr. Build. Mater. 458 (2025) 139444.
[33] Y. Huang, C. Cui, K. Tian, J. Wu, Closed-form solutions for FPR-to-concrete bonded joints with loaded-end anchorage: insight into the interfacial shear transferring mechanism, Structures 66 (2024) 106807.
[34] J.G. Teng, S.T. Smith, J. Yao, J.F. Chen, Intermediate crack induced debonding in RC beams and slabs, Constr. Build. Mater. 17 (6-7) (2003) 447–462.
[35] H. Biscaia, N. Franco, C. Chastre, Stainless steel bonded to concrete: an experimental assessment using the DIC technique, Int. J. Concr. Struct. Mater. 12 (1) (2018) 9.
[36] F.M. Mukhtar, A. Jawdhari, A. Peiris, Mixed-mode FRP-concrete bond failure analysis using novel test apparatus and 3-D non-linear FEM, J. Compos. Constr. 26 (6) (2022).
[37] H.C. Biscaia, T. D'Antino, P. Coelho, F. Conde, Influence of multiple debonding defects on the behaviour of mechanically anchored CFRP-to-steel joints, Compos. Struct. 355 (2025) 118847.
[38] X.L. Zhao, L. Zhang, State-of-the-art review on FRP strengthened steel structures, Eng. Struct. 29 (8) (2007) 1808–1823.
[39] I. Akbar, D.J. Oehlers, M.S.M. Ali, Derivation of the bond–slip characteristics for FRP plated steel members, J. Constr. Steel Res. 66 (8-9) (2010) 1047–1056.
[40] S. Fawzia, X.L. Zhao, R. Al-Mahaidi, Bond-slip models for double strap joints strengthened by CFRP, Compos. Struct. 92 (9) (2010) 2137–2145.
[41] H.T. Wang, G. Wu, Y.T. Dai, X.Y. He, Determination of the bond–slip behavior of CFRP-to-steel bonded interfaces using digital image correlation, J. Reinf. Plast. Compos. 35 (18) (2016) 1353–1367.
[42] J. He, G. Xian, Debonding of CFRP-to-steel joints with CFRP delamination, Compos. Struct. 153 (2016) 12–20.

[43] H.T. Wang, G. Wu, Bond-slip models for CFRP plates externally bonded to steel substrates, Compos. Struct. 184 (2018) 1204–1214.
[44] Y. Doroudi, D. Fernando, H. Zhou, V.T. Nguyen, E. Ghafoori, Fatigue behavior of FRP-to-steel bonded interface: an experimental study with a damage plasticity model, Int. J. Fatigue 139 (2020) 105785.
[45] R. Kalfat, R. Al-Mahaidi, Improvement of FRP-to-concrete bond performance using bidirectional fiber patch anchors combined with FRP spike anchors, Compos. Struct. 155 (2016) 89–98.
[46] E.R. Castillo, R. Kanitkar, Effect of FRP spike anchor installation quality and concrete repair on the seismic behavior of FRP-strengthened RC columns, J. Compos. Constr. 25 (1) (2020).
[47] W. Sun, S. Liu, C. Zhang, An effective improvement for enhancing the strength and feasibility of FRP spike anchors, Compos. Struct. 247 (2020) 112449.
[48] A.S. Bouchikhi, A. Megueni, S. Gouasmi, F.B. Boukoulda, Effect of mixed adhesive joints and tapered plate on stresses in retrofitted beams bonded with a fiber-reinforced polymer plate, Mater. Des. 50 (2013) 893–904.
[49] E. Esmaeeli, P. Shadan, Effectiveness of fan anchors in preventing debonding in FRP-strengthened steel members, Int. J. Steel Struct. 23 (1) (2023) 96–119.
[50] R.Z. Ghaleh, D. Mostofinejad, Behaviour of EBRIG CFRP sheet-concrete joint: comparative assessment with EBR and EBROG methods, Constr. Build. Mater. 346 (2022) 128374.
[51] D. Mostofinejad, S.M. Shameli, Externally bonded reinforcement in grooves (EBRIG) technique to postpone debonding of FRP sheets in strengthened concrete beams, Constr. Build. Mater. 38 (2013) 751–758.
[52] D. Mostofinejad, S.M. Shameli, EBROG and EBRIG methods for strengthening of RC beams by FRP sheets, Eur. J. Environ. Civ. Eng. 18 (6) (2014) 652–668.
[53] N. Moshiri, A. Tajmir-Riahi, D. Mostofinejad, C. Czaderski, M. Motavalli, Experimental and analytical study on CFRP strips-to-concrete bonded joints using EBROG method, Compos. Part B Eng. 158 (2019) 437–447.
[54] D. Mostofinejad, M.H. Mofrad, A. Hosseini, H.H. Mofrad, Investigating the effects of concrete compressive strength, CFRP thickness and groove depth on CFRP-concrete bond strength of EBROG joints, Constr. Build. Mater. 189 (2018) 323–337.
[55] G. Milani, E. Grande, E. Bertolesi, T. Rotunno, M. Fagone, Debonding mechanism of FRP strengthened flat surfaces: analytical approach and closed form solution, Constr. Build. Mater. 302 (2021) 124144.
[56] T. Lu, P. Li, C. Cui, J. Wu, B. Fu, Shear transferring mechanism of the FPR-to-concrete bonded joint with end U-jacketing: a theoretical study, Structures 56 (2023) 104991.
[57] A. Caggiano, E. Martinelli, C. Faella, A fully-analytical approach for modelling the response of FRP plates bonded to a brittle substrate, Int. J. Solids Struct. 49 (17) (2012) 2291–2300.
[58] W.Y. Gao, J.G. Dai, J.G. Teng, Analysis of mode II debonding behavior of fiber-reinforced polymer-to-substrate bonded joints subjected to combined thermal and mechanical loading, Eng. Fract. Mech. 136 (2015) 241–264.
[59] L.A. Nelson, M. Al-Allaf, L. Weekes, Analytical modelling of bond-slip failure between epoxy bonded FRP and concrete substrate, Compos. Struct. 251 (2020) 112596.
[60] H. Biscaia, P. Coelho, F. Conde, T. D'Antino, Theoretical study on the bond performance of CFRP-to-steel single-lap shear tests with multiple debonding defects, Compos. Struct. 345 (2024) 118406.
[61] H.C. Biscaia, The influence of temperature variations on adhesively bonded structures: a non-linear theoretical perspective, Int. J. Non-Linear Mech. 113 (2019) 67–85.
[62] H.C. Biscaia, J. Canejo, S. Zhang, R. Almeida, Using digital image correlation to evaluate the bond between carbon fibre-reinforced polymers and timber, Struct. Health Monit. (2021) 1–24.
[63] T. Carvalho, C. Chastre, H. Biscaia, R. Paula, Flexural behaviour of RC T-beams strengthened with different FRP materials. Third International Fib Congress Washington, 2010.
[64] S&P, S&P Resin 220 HP Epoxy Adhesive, Technical Data Sheet, S&P, Portugal, 2025 (Ref: PT-08.01.26.00).
[65] I. Borba, Comportamento da ligação CFRP/betão em estruturas de betão armado (Master thesis), NOVA School of Science and Technology, 2015 ([in Portuguese]).
[66] Eurocode 2 (EC2), Eurocode 2: design of concrete structures – Part 1-1: general rules ad rules for buildings. EN 1992-1-1, 2004.
[67] H.M. Diab, O.A. Farghal, Bond strength and effective bond length of FRP sheets/plates bonded to concrete considering the type of adhesive layer, Compos. Part B Eng. 58 (2014) 618–624.
[68] A. Moghaddas, D. Mostofinejad, E. Ilia, Empirical FRP-concrete effective bond length model for externally bonded reinforcement on the grooves, Compos. Part B Eng. 172 (2019) 323–338.
[69] A. Li, H. Wang, H. Li, D. Kong, S. Xu, Estimation of bond strength and effective bond length for the double strap joint between carbon fiber reinforced polymer (CFRP) plate and corroded steel plate, Polymers 14 (15) (2022) 3069.
[70] Y. Yang, J. Zhao, S. Zhang, C. Chastre, H. Biscaia, Effect of mechanical anchorage on the bond performance of double overlapped CFRP-to-steel joints, Compos. Struct. 267 (2021) 113902.
[71] H.C. Biscaia, J.G. Dai, An innovative wide-ranging analytical approach for modelling the bond behaviour of frp-to-substrate joints with an elastic end anchorage, Eng. Fract. Mech. 313 (2025) 110662.
[72] M. Aghabagloo, L. Carreras, C. Barris, M. Baena, Experimental investigation on bond behaviour of HB FRP strengthened concrete elements, Compos. Struct. 362 (2025) 119069.
[73] H. Biscaia, N. Carmo, Bond assessment between rebars embedded into a parent material using a single-function bond-slip model, Constr. Build. Mater. 397 (2023) 132396.
[74] P. Rozylo, H. Debski, Failure study of compressed thin-walled composite columns with top-hat cross-section, Thin-Walled Struct. 180 (2022) 109869.
[75] H.T. Wang, Z.N. Bian, M.S. Chen, L. Hu, Q. Wu, Flexural strengthening of damaged steel beams with prestressed CFRP plates using a novel prestressing system, Eng. Struct. 284 (2023) 115953.
[76] J.W. Shi, Q.Q. Wu, B. Li, Y. Liu, W.H. Cao, H.T. Wang, Fatigue bond behavior of FRP-to-concrete joints with various bonding adhesives, Eng. Struct. 301 (2024) 117311.
[77] H. Zhou, C. Yi, Y. Yang, Y. Ou, N. Wang, Bond behavior of CFRP-concrete bonded joints with randomly distributed defects: experimental and numerical studies, Compos. Struct. 369 (2025) 119317.
[78] Hai-Tao Wang, Run-Ze Zhu, M.Zakari Habeeb, Mode-II bonding degradation and debonding of CFRP plate-steel adhesively-bonded interfaces exposed to accelerated water freeze-thaw cycling, Constr. Build. Mater. 482 (2025) 141680.
[79] H.C. Biscaia, Closed-form solutions for modelling the response of adhesively bonded joints under thermal loading through exponential softening laws, Mech. Mater. 148 (2020) 103527.
[80] V. Cervenka, L. Jendele, J. Cervenka, ATENA Program Documentation – Part 1 – Theory, Cervenka Consulting, Prague, 2021 (March).
[81] J. Zhao, G. Liu, Y. Yang, S. Zhang, H. Biscaia, Experimental study on the mixed mode debonding by using a modified CFRP-to-steel double strap joint, Structures 60 (2024) 105874.
[82] D. Shen, X. Shi, Y. Ji, F. Yin, Strain rate effect on bond stress-slip relationship between basalt fiber-reinforced polymer sheet and concrete, J. Reinf. Plast. Compos. 34 (7) (2015) 547–563.
[83] H. Biscaia, R. Almeida, S. Zhang, J. Canejo, Experimental calibration of the bond-slip relationship of different CFRP-to-timber joints through digital image correlation measurements, Compos. Part C Open Access 4 (2021) 100099.
[84] P. Carrara, D. Ferretti, F. Freddi, G. Rosati, Shear tests of carbon fiber plates bonded to concrete with control of snap-back, Eng. Fract. Mech. 78 (15) (2011) 2663–2678.
[85] K. Dong, Y. Gao, S. Yang, Z. Yang, J. Jiang, Experimental investigation and analytical prediction on bond behaviour of CFRP-to-concrete interface with FRP anchors, Case Stud. Constr. Mater. 19 (2023) e02510.
[86] J.Q. Yang, S.T. Smith, Z. Wang, Y.Y. Lim, Numerical simulation of FRP-strengthened RC slabs anchored with FRP anchors, Constr. Build. Mater. 172 (2018) 735–750.